Mon. Not. R. Astron. Soc. **000**, 000–000 (0000) Printed 12 July 2011 (MN LATEX style file v2.2)

The Role of Dissipation in the Scaling Relations of Cosmological Merger Remnants

M. D. Covington[1,2,3], J. R. Primack[1,2⋆], L. A. Porter[1,2], D. J. Croton[4], R. S. Somerville[5,6], and A. Dekel[2,7]

[1] *Department of Physics, University of California, Santa Cruz, California 95064, USA*
[2] *Santa Cruz Institute for Particle Physics, University of California, Santa Cruz, California 95064, USA*
[3] *NSF International Research Fellow, Karst Research Institute ZRC SAZU, Titov trg 2, SI-6230 Postojna, Slovenia*
[4] *Centre for Astrophysics and Supercomputing, Swinburne University of Technology, Melbourne, Australia*
[5] *Space Telescope Science Institute, 3700 San Martin Drive, Baltimore, Maryland 21218, USA*
[6] *Department of Physics and Astronomy, Johns Hopkins University, Baltimore, Maryland 21218, USA*
[7] *Racah Institute of Physics, The Hebrew University, Jerusalem, 91904, Israel*

12 July 2011

ABSTRACT

There are strong correlations between the three structural properties of elliptical galaxies – stellar mass, velocity dispersion and size – in the form of a tight "fundamental plane" and a "scaling relation" between each pair. Major mergers of disk galaxies are assumed to be a mechanism for producing ellipticals, but **semi-analytic galaxy formation models (SAM) have** encountered apparent difficulties in reproducing the observed slope and scatter of the size-mass relation. We study the scaling relations of merger remnants using progenitor properties from two SAMs. We apply a simple merger model that includes gas dissipation and star formation based on theoretical considerations and simulations. **Combining the SAMs and the merger model allows calculation of the structural properties of the remnants of major mergers that enter the population of elliptical galaxies at a given redshift.** Without tuning the merger model parameters for each SAM, the results roughly match the slope and scatter in the observed scaling relations and their evolution in the redshift range $z = 0 - 3$. Within this model, the observed scaling relations, including the tilt of the fundamental plane relative to the virial plane, result primarily from the decrease of gas fraction with increasing progenitor mass. The scatter in the size-mass relation **of the remnants** is **reduced from that of the progenitors** because of a correlation between progenitor size and gas fraction at a given mass.

Key words: galaxies: interactions – galaxies: evolution – galaxies: elliptical and lenticular, cD – galaxies: formation – methods: .

1 INTRODUCTION

The merging of disk galaxies is one of the main hypothesized mechanisms for the formation of elliptical galaxies. Simulations have shown that mergers of disks with similar masses can effectively disrupt the ordered rotation in the disks and convert it into random velocity support, creating merger remnants that appear similar to observed elliptical galaxies (Toomre & Toomre 1972; Toomre 1977; Barnes & Hernquist 1992; Mihos & Hernquist 1994). Furthermore, the ΛCDM cosmology predicts the hierarchical buildup of galaxies through a sequence of mergers. These results suggest that merging is a likely mechanism for the production of elliptical galaxies.

However, observed ellipticals follow a number of scaling relations, including relatively tight relations between stellar mass and velocity dispersion, the Faber-Jackson relation (Faber & Jackson 1976), and between size and stellar mass (Kormendy 1977). Furthermore, observed ellipticals fall on a tight plane, the fundamental plane (FP), in the three-dimensional space of stellar mass, size, and velocity dispersion (Djorgovski & Davis 1987; Dressler et al. 1987). Recent studies of the Sloan Digital Sky Survey (SDSS) have provided excellent statistics on these scaling relations in the local universe (Shen et al. 2003; Bernardi et al. 2003a,b; Padmanabhan et al. 2004; Gallazzi et al. 2006;

⋆ email: joel@scipp.ucsc.edu

Shankar et al. 2010), and studies using high redshift surveys have provided evidence for the evolution of these relations over cosmological time (Barden et al. 2005; McIntosh et al. 2005; Trujillo et al. 2006; Trujillo et al. 2007; Cimatti et al. 2008; van der Wel et al. 2008; Buitrago et al. 2008; Saracco et al. 2009; van Dokkum et al. 2010; Fan et al. 2010; Mancini et al. 2010; Williams et al. 2010). If mergers are a major mechanism for the production of elliptical galaxies then they must be able to produce the correct scaling relations as well as the evolution of these scaling relations over time. Theoretical **high-resolution, hydrodynamical** studies have shown that simulations of gas-rich galaxy mergers are capable of reproducing the observed scaling relations of elliptical galaxies if the correct progenitor properties are used (Dekel & Cox 2006; Robertson et al. 2006; Hopkins et al. 2008; Bournaud et al. 2011). **These studies have been successful in creating high-redshift compact ellipticals from major mergers of gas-rich compact disk galaxies (Bournaud et al. 2010; Wuyts et al. 2010).** This is a step toward verifying the production of scaling laws through mergers. However, current computing power only allows the simulation of relatively small numbers of mergers, and the space of possible merger initial conditions and progenitor properties is quite large. Furthermore, these simulations are not placed within a cosmological context, making it more difficult to explore in detail the origin and evolution of scaling relations.

Currently, the primary theoretical tool for studying the evolution of statistical samples of galaxies over cosmological timescales is semi-analytic modeling (SAM) (Kauffmann et al. 1993; Cole et al. 1994; Somerville & Primack 1999; Cole et al. 2000; Hatton et al. 2003; Croton et al. 2006; De Lucia et al. 2006; Bower et al. 2006; Somerville et al. 2008; Fontanot et al. 2009; Benson 2010; Benson & Bower 2010; Cook et al. 2010; Guo et al. 2010). These models combine dark matter halo merger trees with analytic recipes for populating the halos with galaxies. However, semi-analytic models (SAMs) do not currently incorporate realistic formulas for predicting the properties of the remnants of galaxy mergers including the effects of dissipation. The agreement between current SAMs and observed early-type scaling relations is not impressive. In particular, the observed size-mass relation of early-types is steeper than that of their potential late-type progenitors (Shen et al. 2003), and the scatter in the observed size-mass relation for early-types is remarkably small (Shen et al. 2003; Nair et al. 2010). The disspationless merger models currently implemented within SAMs have thus far been unable to reproduce these features (e.g., Shankar et al. 2010; Guo et al. 2010). **Using a simple power law dissipation model Khochfar & Silk (2006) were able to reproduce the redshift-size evolution of elliptical galaxies, which, along with the high-resolution hydrodynamical simulations described above, suggests that dissipative effects may play an important role in determining elliptical galaxy scaling relations.**

Covington et al. (2008) recently developed a physically-motivated analytic model for predicting the stellar half-mass radii and central velocity dispersions of merger remnants (Covington et al. 2008). The parameters in this new merger model were calibrated using a suite of **high-resolution hydrodynamical** galaxy merger simulations (see Section 2). Here we implement a simplified version of this model using post-processing of merger outputs from the SAMs developed by Croton et al. (2006), based on the Millennium simulation (Springel et al. 2005), and Somerville et al. (2008). This results in a population of tens of thousands of merger remnants over a large range of redshifts ($0 < z < 3$) complete with predicted values of size, stellar mass, and velocity dispersion. Comparison of the modeled population of ellipticals with the observed scaling relations provides an important test of the merger hypothesis as well as physical insight into the origin and evolution of these relations via merging. **It is important to note that the model presented here is calibrated only for major mergers of disk-dominated galaxies, and that we make no attempt to model subsequent evolution following the formative major merger.** Future work will **expand our model to include minor mergers and mergers of bulge-dominated galaxies. We will also** implement our merger model self-consistently within the semi-analytic machinery rather than by post-processing.

Section 2.1 describes our analytic merger model for calculating the properties of stellar spheroids from galaxy mergers including energy losses from dissipation. Section 2.2 explains how we implement our merger model using outputs from the Croton et al. (2006) and Somerville et al. (2008) SAMs. Section 3 systematically explores the effects of the merger model. In order to turn the rather shallow size-mass relation of disk galaxies into the steeper size-mass relation of observed early-type galaxies, we find that it is essential to include both dissipation and the decreasing gas content of more massive progenitor disk galaxies. In Section 4 we summarize the observational results that we compare with our model outputs, focusing especially on Sloan Digital Sky Survey (SDSS) data for nearby galaxy size vs. mass and other scaling relations, and on data from several surveys (Trujillo et al. 2006) for the evolution of these relations to higher redshifts. In section 5 we use the predicted properties of progenitor disk galaxies from the two semi-analytic models to predict the size-mass and other relations for spheroids formed in major gas-rich mergers and compare them with the observations out to redshift $z = 3$. Section 6 summarizes these results and discusses their implications and some follow-on studies that are in progress. Finally, an Appendix describes an improvement in the treatment of the central dark matter in the analytic merger model of Covington et al. (2008) that we used in Covington (2008) and in the present paper.

2 METHODOLOGY

We use a combination of modeling approaches to construct a theoretical framework for predicting the evolution of early-type scaling relations over cosmological time. In previous work, a large suite of hydrodynamical galaxy merger simulations were developed (Cox 2004; Cox et al. 2006, 2008). These simulations were performed using the N-body/SPH code GADGET (Springel et al. 2001; Springel & Hernquist 2003), and include hydrodynamics, star formation, and stellar feedback. The simulation suite contains mergers with a wide variety of progenitor properties, mass ratios, and merger orbits. Variations in progenitor properties include

a range of stellar masses, gas fractions, dark matter halo concentrations, bulge fractions, baryonic fractions, and gas disk sizes.

In subsequent work, Covington et al. (2008, hereafter C08) constructed a physically-motivated analytic galaxy merger model capable of predicting the half-mass radii, stellar masses, and velocity dispersions of galaxy merger remnants given the properties of the **disk** progenitor galaxies and the initial orbits of the mergers. This model was calibrated using the galaxy merger suite described above. Unlike previous similar models (Cole et al. 2000; Hatton et al. 2003), this model includes the effects of star formation and energy loss due to dissipation. Here we combine a simplified version of this new galaxy merger model with merger rates and progenitor properties predicted by two semi-analytic models (SAMs) in order to explore the creation and evolution of the scaling relations of early-type galaxies.

2.1 Description of the Merger Model

Previous models for predicting the sizes and velocity dispersions of galaxy merger remnants employed a combination of energy conservation and the virial theorem (Cole et al. 2000; Hatton et al. 2003). Assuming homology between progenitors and remnants then allows a straightforward calculation of remnant properties. However, the most common mergers at higher redshifts are 'wet' mergers of gaseous galaxies, and the approach used previously does not account for energy losses due to gas processes. Recent work has suggested that these dissipative effects play an important role in the formation of elliptical galaxies (Cox et al. 2006; Robertson et al. 2006; Dekel & Cox 2006; Ciotti et al. 2007; Cox et al. 2008; Hopkins et al. 2008)**, though there is also evidence that disks may preserved in major, gas-rich mergers (Springel & Hernquist 2005; Robertson et al. 2006; Hopkins et al. 2009)**. C08 develops a framework for modifying the energy conservation approach to include dissipative losses due to gas processes.

In order to account for dissipative losses, we include a radiated energy term within the energy conservation equation. Furthermore, since stars form during the merger, we include the mass of gas that will form stars when calculating the internal energies of the progenitor galaxies. C08 found that the energy lost and the number of new stars formed are a function of both the gas fraction and the initial merger orbit. Closer, more disruptive encounters will result in greater total energy losses and larger numbers of stars forming. However, the set of orbital parameters in the simulations used to calibrate the model was not intended to be statistically representative of mergers in the real Universe. Rather, it was intended to sparsely span the range of reasonable values. In the present work, we find that when the merger model of C08 is applied to SAMs using the distribution of merger orbital parameters observed in cosmological N-body simulations (Benson 2005) there is relatively small scatter in remnant properties as the result of orbit. Consequently, for this paper we use a simplified version of the model in C08 where remnant properties are not a function of orbit. This simplified model is calibrated to the same suite of galaxy merger simulations (Cox 2004), effectively averaging over the range of orbits within the suite.

Additionally, the model for calculating remnant central dark matter fractions developed in C08, when applied within SAMs, fails for a subset of cases with large radii and high gas fractions. Therefore, here we use a new model for calculating central dark matter fractions that has a broader range of applicability (see Appendix A for details). Together, the modifications described result in a simpler model that captures the core dynamics of the more complicated model of C08. This has the added benefit of reducing the number of unknown model parameters. However, the scaling relations produced by the two models are not identical, and further work now underway implementing these models within SAMs will be needed to determine whether the simpler model presented here is sufficient (see Section 5.3 for a discussion of differences).

The first step in the new model is to calculate the star formation efficiency of the merger, e. Following Somerville et al. (2001) we use

$$e = e_{1:1}\left(\frac{M_{\rm sat}}{M_{\rm primary}}\right)^{\gamma}. \quad (1)$$

This formula was calibrated to our merger simulations in Cox et al. (2008) resulting in parameter values of $e_{1:1} = 0.55$ and $\gamma = 0.69$. For each merger $M_{\rm sat}$ is taken to be the total mass (dark matter plus baryons) of the less massive progenitor and $M_{\rm primary}$ is taken to be the total mass of the more massive progenitor. For each progenitor

$$M_{\rm ns} = eM_{\rm gas}, \quad (2)$$

where $M_{\rm ns}$ is the mass of new stars formed in the merger and $M_{\rm gas}$ is the initial (cold) gas mass of the progenitor.

As in C08, we use an energy conservation equation to calculate the half-mass radius of the merger remnant. This equation includes final and initial internal energy terms and a term for energy loss due to gas dissipation,

$$E_{\rm final} = E_{\rm init} + E_{\rm rad}. \quad (3)$$

The energy terms are calculated as follows:

$$E_{\rm init} = G\left(\frac{(M_{\rm s,1}+M_{\rm ns,1})^2}{R_1} + \frac{(M_{\rm s,2}+M_{\rm ns,2})^2}{R_2}\right), \quad (4)$$

$$E_{\rm final} = G\frac{(M_{\rm s,1}+M_{\rm ns,1}+M_{\rm s,2}+M_{\rm ns,2})^2}{R_{\rm final}}, \quad (5)$$

and

$$E_{\rm rad} = C_{\rm rad}f_{\rm g}E_{\rm init}, \quad (6)$$

where $M_{\rm s,i}$ is the initial stellar mass of progenitor i, $R_{\rm i}$ is the initial 3D **stellar** half-mass radius of progenitor i, and $R_{\rm final}$ is the 3D **stellar** half-mass radius of the remnant. $C_{\rm rad} = 2.75$ is a constant parameter calibrated using the merger simulations, and

$$f_{\rm g} = \frac{M_{\rm g,1}+M_{\rm g,2}}{M_{\rm s,1}+M_{\rm g,1}+M_{\rm s,2}+M_{\rm g,2}} \quad (7)$$

is the merger gas fraction **where $M_{\rm s,i}$ and $M_{\rm g,i}$ are the stellar and gas masses, respectively, of the progenitors. Unlike in C08, here orbital energy is neglected, because we find that, using orbital parameters observed in cosmological N-body simulations (Benson 2005), the scatter resulting from orbital effects is small. In the limit of no dissipation (i.e.$f_{\rm g} = 0$), Eqs. 3-5 in our paper reduce to Eqs. 1 and 2 of Naab**

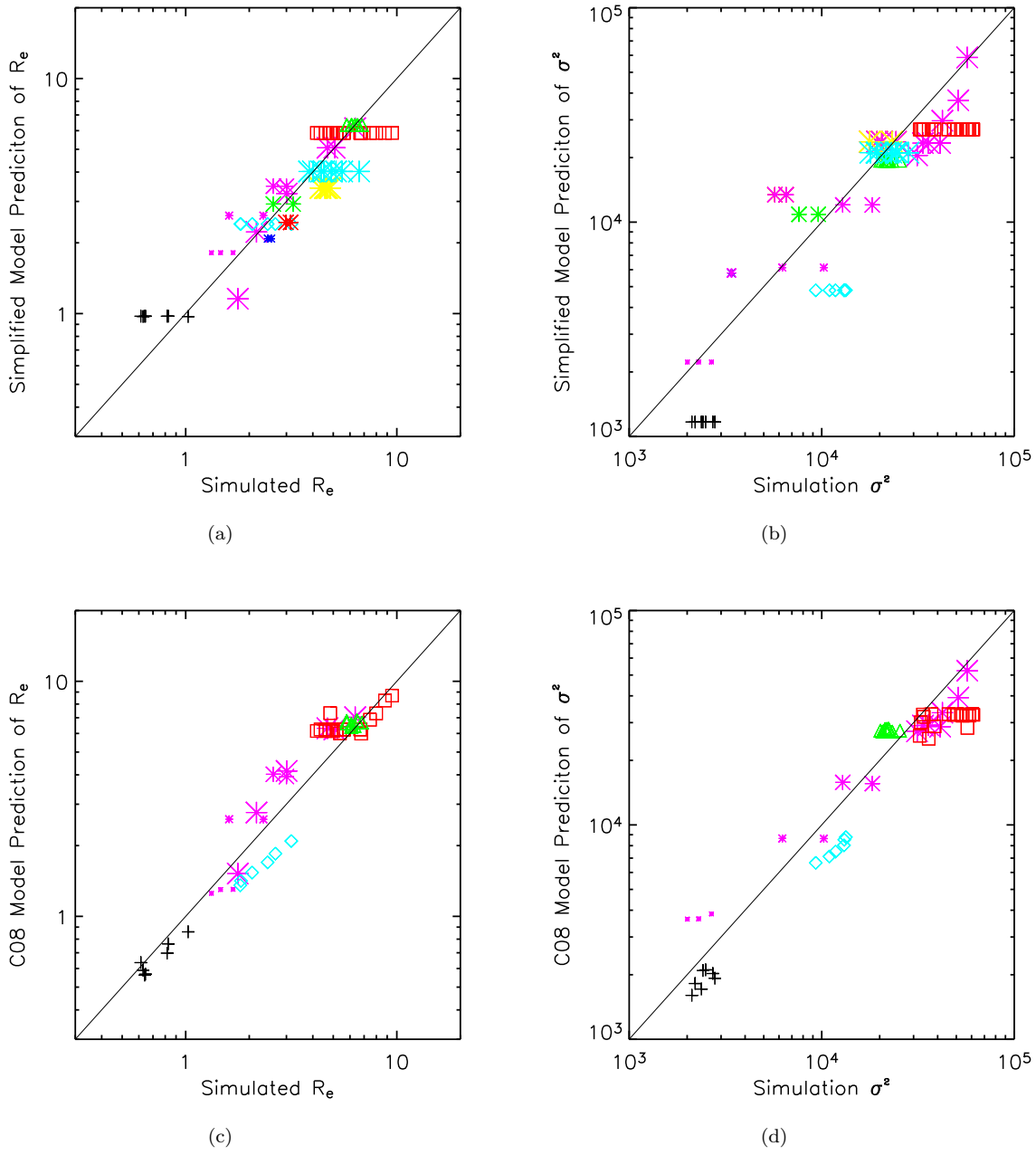

Figure 1. Half-mass radii of merger remnants from our simulation suite plotted against radii predicted from our simplified analytic merger model, (a), and the full C08 model with central dark matter density calculated as in Appendix A (c). Panels (b) and (d) show the predictions for velocity dispersions for the simple model and C08 plus Appendix A, respectively. Different symbols represent different types of progenitor galaxies, **described in detail in C08**. This new, simpler merger model does not capture variations due to initial orbit, **which is seen in the horizontal spread within symbols of the same size, shape, and color,** but we find that the spread resulting from this mechanism is insignificant when drawing orbits from the distribution observed in N-body simulations. The simple model was calibrated with a few more simulations that were not available during the initial calibration in C08.

et al. (2009), if one assumes the proportionality of effective and gravitational radii as we do here.

Once we have calculated the final radius, we can compute the velocity dispersion. First, we calculate the central dark matter fraction of the merger remnant, $f_{\rm dm,f}$ (see Appendix A for details). Then, as in C08, we calculate the remnant velocity dispersion using the virial relation,

$$\sigma^2 = \frac{GC_{\rm sig}M_{\rm s,f}}{R_{\rm f}(1-f_{\rm dm,f})}. \quad (8)$$

$M_{\rm s,f}$ is the stellar mass of the remnant, and $C_{\rm sig} = 0.15$ is a constant parameter fit to the simulations.

In order to determine the parameters $C_{\rm rad}$ and $C_{\rm vir}$, we calculated a best-fit of the model to the merger remnants in our simulation suite. The fit of the new model is depicted

in Figure 1a-b, while the results from the C08 model with the modified calculation of central dark matter fraction are shown in panels c and d. On average, the new model correctly predicts the remnant sizes and velocity dispersions. However, there is more spread in the accuracy of predictions in the simple model. This results from variations in initial orbit in our simulation suite. **As stated above, we find that this variation is insignificant when mergers are calculated for the distribution of orbits found in cosmological N-body simulations.**

We note that our merger model has primarily been calibrated for major mergers of disk-dominated galaxies. An expansion of this model that includes a detailed treatment of minor mergers and mergers of elliptical galaxies is forthcoming (Porter et al., in prep), but here we do not attempt to model subsequent evolution of elliptical galaxies following the initial major merger because the current versions of the SAMs do not track bulge sizes using our dissipative model. In limiting our model to major mergers, we are only examining one avenue of elliptical galaxy formation. Recent works (Naab et al. 2006; Bournaud et al. 2007) have suggested that ellipticals can also form as a product of minor mergers, but we do not attempt to model this here.

2.2 Implementation of Merger Model with SAMs

In order to make comparisons with observational data, and to explore the evolution of scaling relations over cosmological time scales, we apply the new merger model to progenitor properties from two SAMs: the Somerville et al. (2008) SAM (hereafter S08) and a SAM based on the Millennium Simulation (Croton et al. 2006). We implement the merger model externally (i.e., by post-processing) rather than incorporating it within each of the SAMs. This provides an expedient means of exploring the properties of new elliptical galaxies arriving into the population via the merging of disk-dominated galaxies. We restrict our analysis to mergers of disk galaxies because the current generation SAMs do not have a reliable method for calculating bulge sizes, and we need stellar radii in order to calculate initial internal energies. Furthermore, **since the merger suite was designed to model mergers of disk galaxies, there were few bulge-dominated progenitors used to calibrate the merger model. The performance of the model for mergers of bulge-dominated galaxies has not been tested.** Consequently, we only analyze mergers in each SAM where both progenitors have a stellar disk more massive than their bulge. Additionally, since we are comparing the remnants to observations of elliptical galaxy populations, we only include major mergers with a mass ratio of 1:3 or greater, as these are the mergers expected to create elliptical galaxies.

Each SAM directly provides the stellar mass, disk radius, and mass of cold gas for each progenitor. In addition, the model requires information about the dark matter halo of each progenitor galaxy. Specifically, we need to be able to calculate mass as a function of radius in order to calculate both the halo half-mass radius and the central dark matter mass. S08 and Millennium provide the masses of the dark matter halos, but specify the halo mass distributions using different quantities. S08 provides halo concentrations. The Millennium SAM provides $V_{\rm max}$ and $V_{\rm vir}$, from which concentration can be calculated. For both cases the concentration, virial mass, and redshift are used to calculate the distribution of mass within the halo. For S08 the spherical top-hat collapse model is used to calculate the virial overdensity, using the approximation from Bryan & Norman (1998), whereas for Millennium the virial overdensity is assumed to be 200. All of these calculations assume the ΛCDM concordance cosmology, with $\Omega_{\rm m} = 0.3$, $\Omega_\Lambda = 0.7$, and $h = 0.7$.

3 SYSTEMATIC EXPLORATION OF THE MERGER MODEL

To gain a better intuitive grasp of the behavior of the merger model, we systematically explore the effects of variations in the progenitor properties and model parameters. For this study we introduce a series of four idealized progenitor galaxy models. In order to isolate the effects of various progenitor properties we begin with a fiducial progenitor and scale the progenitor properties in such as way as to keep baryon fraction, average density, and halo concentration constant.

The fiducial galaxy with which we begin our series is the G3 galaxy from Cox et al. (2008), whose properties are designed to fit the average properties of observed nearby disk galaxies in the Sloan Digital Sky Survey. The G3 has a dark matter halo mass of $1.1 \times 10^{12} {\rm M}_\odot$, a stellar mass of $5.0 \times 10^{10} {\rm M}_\odot$, an initial half-mass radius of 3.8 kpc, and a halo concentration of 6.0. Each subsequent galaxy in the series is created by reducing the mass by 1/3, keeping the average densities, concentration, and baryon fraction constant**, and calculating σ using the virial theorem.**

3.1 Effect of Varying Gas Fraction with Mass

Previous work has shown that gas can have a significant effect on merger remnants (Barnes & Hernquist 1996; Robertson et al. 2006; Dekel & Cox 2006; Springel & Hernquist 2005; Naab et al. 2006). Dekel & Cox (2006) suggest that a systematic variation in gas fraction with mass could be responsible for the tilt in the fundamental plane of elliptical galaxies, and Hopkins et al. (2008) demonstrate observational evidence for this hypothesis. Thus, we examine the effect of progenitor gas fraction, defined here as the ratio of gas to stellar mass, on the properties of equal-mass merger remnants.

In our first experiment we set the gas mass of each progenitor such that gas fraction is constant as a function of mass. We run the model for several gas fractions, setting the ratio of gas mass to stellar mass to 0.0, 0.25, 0.5, 1.0, and 2.0. The size-stellar mass relation, stellar-mass Faber-Jackson relation (FJ), and virial projection of the fundamental plane (FP) of the merger remnants are shown in Figure 2(a).

Several observations are worth noting about the size-mass relations plotted in Figure 2(a). First, for all gas fractions the remnant relations (crosses) are just shifted horizontally and vertically from the progenitor relation (stars) without any significant rotation (i.e., change of slope). That is, the vector between progenitor and remnant is constant

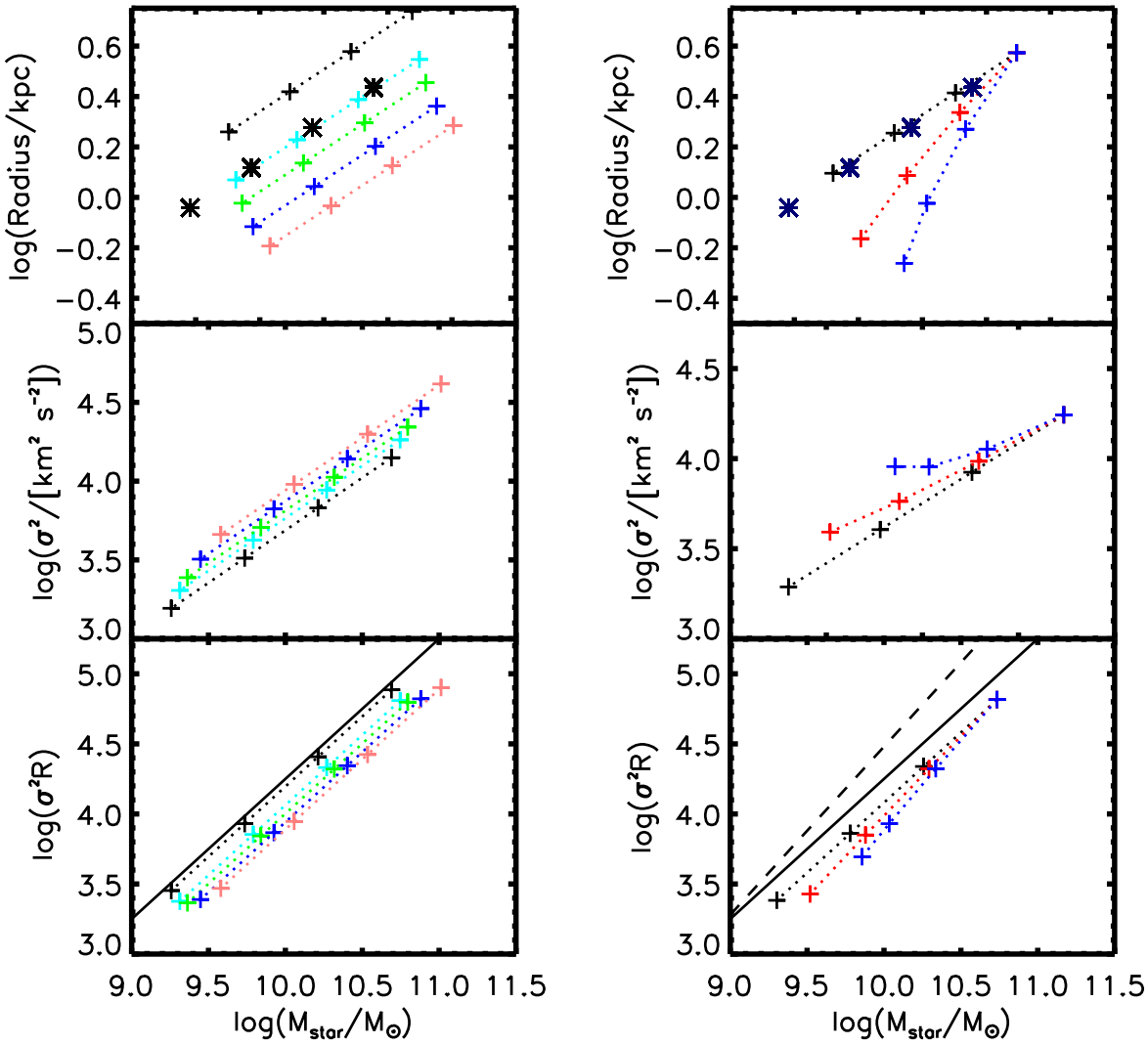

Figure 2. Scaling relations for **1:1** merger remnants produced by our model using **a series of idealized progenitors of different mass**. The progenitors used in (a) have a range of initial gas fractions, which are held constant as a function of mass. For remnants, colors depict ratio of gas mass to stellar mass in the progenitors that created that remnant where black=0.0, light blue=0.25, green=0.5, blue=1.0, and red=2.0. Dotted lines connect remnants **resulting from** progenitors with **different mass but** the same gas fraction. The progenitors used in (b) have gas fractions that vary as a power law of baryonic mass ($M_{\rm gas}/M_{\rm baryons} \propto M_{\rm baryons}^{-\gamma}$). For remnants, colors depict the value of γ used to set the progenitor gas fractions black=0.0, red=0.5, and blue=1.0. Dotted lines connect remnants with progenitors from the same gas fraction power law. The top panels show the size-stellar mass relation of the merger remnants (crosses) and progenitors (stars), while the middle and lower panels show the stellar mass FJ relation and the fundamental plane for the merger remnants, respectively. The solid line plotted in the lowest panels shows the slope for galaxies with a virial scaling, whereas the dashed line shows the observed tilt in the FP. Steepening in the size-mass relationship and tilt in the FP are produced by a decreasing gas fraction with increasing baryonic mass.

for any given gas fraction. This means that $R_{\rm f}/R_{\rm i}$ and $M_{\rm star,f}/M_{\rm star,i}$ are also constant for any particular gas fraction. This is worth noting because the observed size-mass relations for disks and ellipticals are significantly rotated from one another with the relation for ellipticals being much steeper. A realistic mechanism for the production of ellipticals must account for this steepening.

Remember that the progenitors are constructed so that they have a constant density inside their half-mass radius. Thus one can quickly see from the plot that 'dry' mergers, with no gas, will produce remnants with densities less

than their progenitors and sizes larger than their progenitors, whereas gas-rich mergers will produce remnants with densities higher than their progenitors. The sizes of the remnants of gas-rich mergers can be similar to or even smaller than the sizes of their progenitors. For this set of model parameters, constant density evolution occurs at roughly a gas-to-stellar-mass ratio of 0.25 (light-blue crosses).

The stellar-mass FJ plot, in the second panel of Figure 2(a), demonstrates a similar effect. Progenitors are not shown because they have no values for σ, however one can see that remnants of mergers with each gas fraction follow parallel lines. No rotation is introduced between one gas fraction series and the next.

If elliptical galaxies followed an exact virial relation, then one would expect that $M_{\rm star} \propto \sigma^2 R$. Thus plotting these quantities against each other gives us a 'virial' projection of the fundamental plane. Galaxies following the virial relation would fall on a line with a slope of one. Observed galaxies do not fall on the expected virial relation. This variance from virial scaling is the so-called tilt of the fundamental plane. In the third panel of Figure 2(a) we plot $M_{\rm star}$ versus $\sigma^2 R$. The line plotted has a slope of one and therefore follows a virial scaling. The remnants from each gas fraction set fall on the same virial scaling. This demonstrates that our model produces no tilt in the fundamental plane for remnants when the progenitors' properties are scaled with the mass. However, while each gas fraction series follows the virial scaling, there is a shift between cases with different gas fractions such that larger gas fraction progenitors result in remnants with larger ratios of stellar mass to dynamical mass.

In the next experiment we let gas fraction vary as a function of mass. We fix the gas mass of the largest progenitor (G3) such that the ratio of gas mass to stellar mass is 0.25. Then we let the baryonic gas fraction vary as a power law with the baryonic mass, $M_{\rm gas}/M_{\rm baryons} \propto M_{\rm baryons}^{-\gamma}$ (as suggested in Dekel & Cox (2006)). We use values of γ equal to 0, 0.5, and 1.0. In Figure 2(b) we show the scaling relations of the remnants produced by this series of progenitors. Each line of remnants is fixed to the largest mass remnant, but the slope of the size-mass and FJ relations clearly depends on the value chosen for γ. Non-zero values of γ allow for significant rotations in all of the plotted projections of the FP. The rotation in the size-mass relation is the direction of rotation required if one is to create ellipticals from mergers of disks that follow the observed relations. Additionally, the fundamental plane relation rotates away from the virial relation in the same direction as the observed tilt. For reference, the slope of the observed tilt is shown with a dashed line. The tilt required is slightly overshot by the $\gamma = 1$ case, suggesting that a slightly shallower power law slope would reproduce the observed tilt. This result is compatible with the gas fraction power of 0.7 suggested by Dekel & Cox (2006). Thus within our model a gas fraction gradient is capable of creating a tilt in the fundamental plane.

Our model relies on the virial relation to calculate sizes and velocity dispersion. However, in our model the central dark matter fraction is calculated assuming that no dissipation occurs within the dark matter halo, and this affects our calculation of σ. The break from virial scaling results from this changing central dark matter fraction, with more gas rich progenitors producing a larger difference between the dissipational baryons and dissipationless dark matter resulting in a lower central dark matter fraction.

For large values of γ some curvature is also introduced into the scaling relations. Since both the disk and elliptical scaling relations are approximately power laws, this puts a constraint on the strength of the gas fraction variation allowed by the model if we want to reproduce the observed scaling relations. However, the expected value of $\gamma = 0.7$ only produces a modest amount of curvature.

3.2 Merger Model Parameters

The merger model contains several parameters with uncertain values because of the uncertainty in the feedback prescription used by the merger simulations. Because of this uncertainty, the values of the model parameters might require adjustment. In order to understand the effect of these parameters we vary them systematically and examine the results of these variations on the remnant scaling relations.

We begin by varying the star formation efficiency parameter, $e_{1:1}$. The calibrated value of this parameter (from the simulations) is 0.55, but for the experiments below we use values of 0.1, 0.5, and 1.0. First, we assume a constant gas-to-stellar-mass ratio of 0.5 across the idealized galaxy series. Increasing $e_{1:1}$ will increase the number of stars that form; however, it has little effect on the remnant scaling relations (Figure 3(a)). Specifically, none of the relations experience significant rotation as a result of the adjustment. For all relations an increase in $e_{1:1}$ simply results in a slight shift toward higher stellar mass.

For the second experiment with $e_{1:1}$, we introduce a mass-dependent gas fraction according to the power law relation used above, using the expected value of $\gamma = 0.7$. For this series, adjusting $e_{1:1}$ produces rotations of the scaling relations. Specifically, changing $e_{1:1}$ has a greater effect on the mergers with a larger gas fraction, resulting in rotations in the size-mass and FJ relations and a slight tilting in the FP (Figure 3(b)).

Another parameter for which feedback could produce some uncertainty is $C_{\rm rad}$, which sets the importance of the radiative energy term. Since the $C_{\rm rad}$ parameter is decoupled from the equation that determines the number of new stars, adjusting $C_{\rm rad}$ results in no difference in final mass. However, an increase of the parameter results in a significant reduction of size and increase in velocity dispersion for the remnants. The same constant gas fraction and mass-dependent gas fraction merger series used for the star formation parameter series are plotted in Figures 4(a) and 4(b), respectively, with $C_{\rm rad}$ taking values of 1.0 (black), 3.0 (red) and 5.0 (blue). The value of $C_{\rm rad}$ determined by fitting to the merger simulations was 2.75. As with $e_{1:1}$, rotation in the scaling relations is only seen for the series with a mass-dependent gas fraction. Here, a significant rotation is created in the size-mass and FJ relations, but adjusting $C_{\rm rad}$ never introduces a tilt in the FP. This is because the model is built on the assumption of the virial theorem, and the only portion of the model that violates this assumption is the formula for calculating the change in central dark matter fraction, which is then used to adjust the velocity dispersion. Changing $C_{\rm rad}$ does not affect this portion of the model.

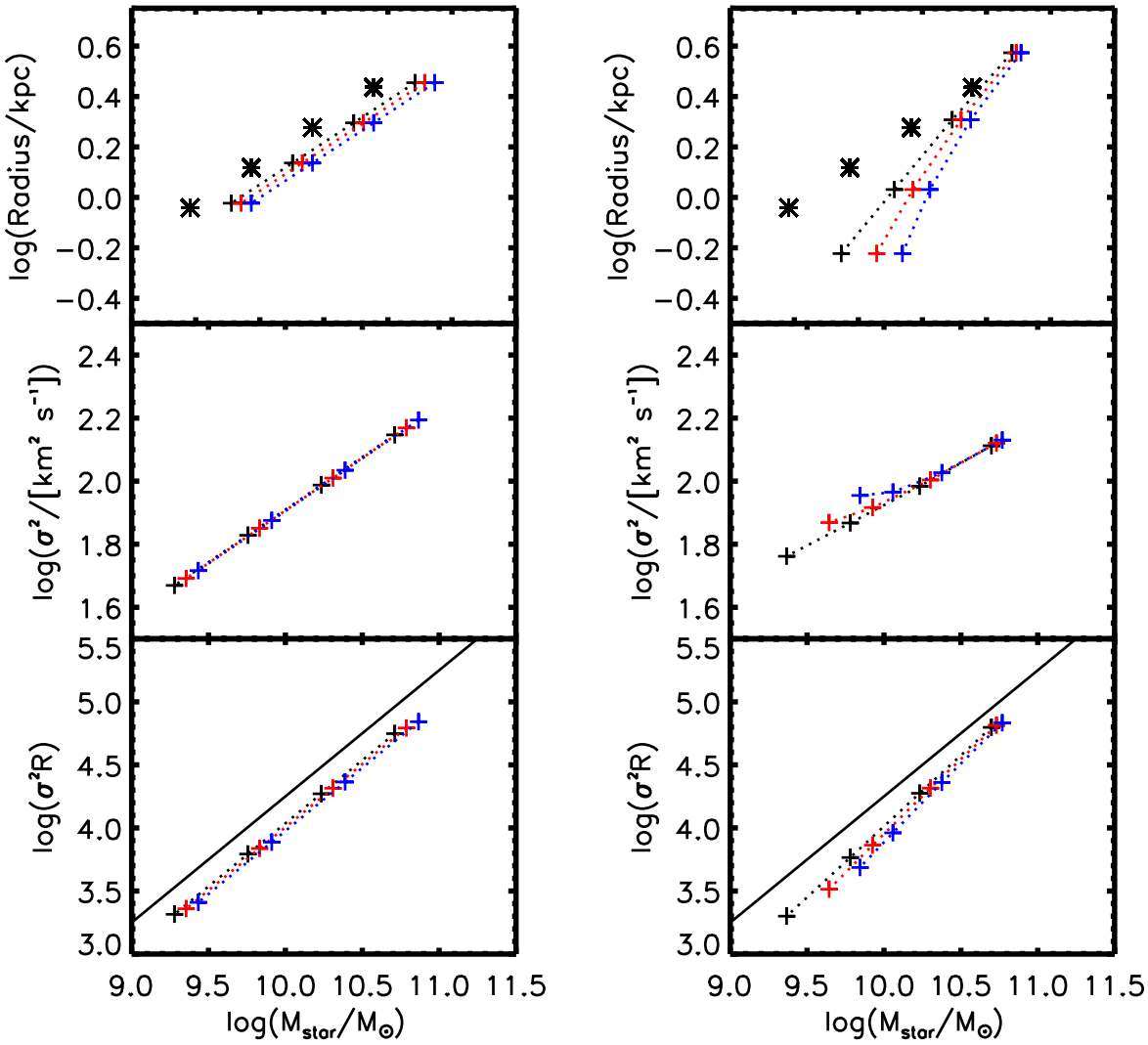

Figure 3. Scaling relations for merger remnants produced by the model from our series of idealized progenitors with varying star formation parameter $e_{1:1}$, which takes values of 0.1 (black), 0.5 (red), and 1.0 (blue). 0.55 is the calibrated value. Dotted lines connect cases with the same value of $e_{1:1}$. Progenitors in (a) have a constant gas to stellar mass ratio of 0.5, whereas progenitors in (b) have a changing gas fraction with mass ($\gamma = 0.7$). The top panels show the size-stellar mass relation of the merger remnants (crosses) and progenitors (stars), while the middle and lower panels show the stellar mass FJ relation and the fundamental plane for the merger remnants, respectively. The solid line plotted in the lowest panels shows the FP slope for galaxies with a virial scaling. Changing $e_{1:1}$ affects the slopes of all three scaling relations, but only when gas fraction varies as a power law of stellar mass (b).

4 SUMMARY OF OBSERVATIONAL RESULTS

The Sloan Digital Sky Survey (SDSS) (York et al. 2000) has provided exquisite statistics on galaxy scaling relations in the local universe. Shen et al. (2003) show that for local galaxies the size distribution for each type of galaxy at a given stellar mass is log-normal. They provide fitting functions for the medians of the distributions for both early- and late-type galaxies. For late-type galaxies the median ($\bar{R}$) is described by

$$\bar{R}(\mathrm{kpc}) = \gamma \left(\frac{M}{\mathrm{M}_\odot}\right)^{\alpha} \left(1 + \frac{M}{M_0}\right)^{\beta-\alpha}, \quad (9)$$

where $\gamma = 0.1$, $\alpha = 0.14$, $\beta = 0.39$, and $M_0 = 3.98{\times}10^{10}\mathrm{M}_\odot$. A comparison of this distribution to that of Barden et al. (2005), also from SDSS, demonstrates a discrepancy, despite the fact that the samples contain significant overlap. Specifically, a comparison of the stellar-mass size ridge line in Somerville et al. (2008) with the figure in Shen et al., correcting for the conversion between disk scale length and half light radius, shows that the Shen et al. distribution is a fac-

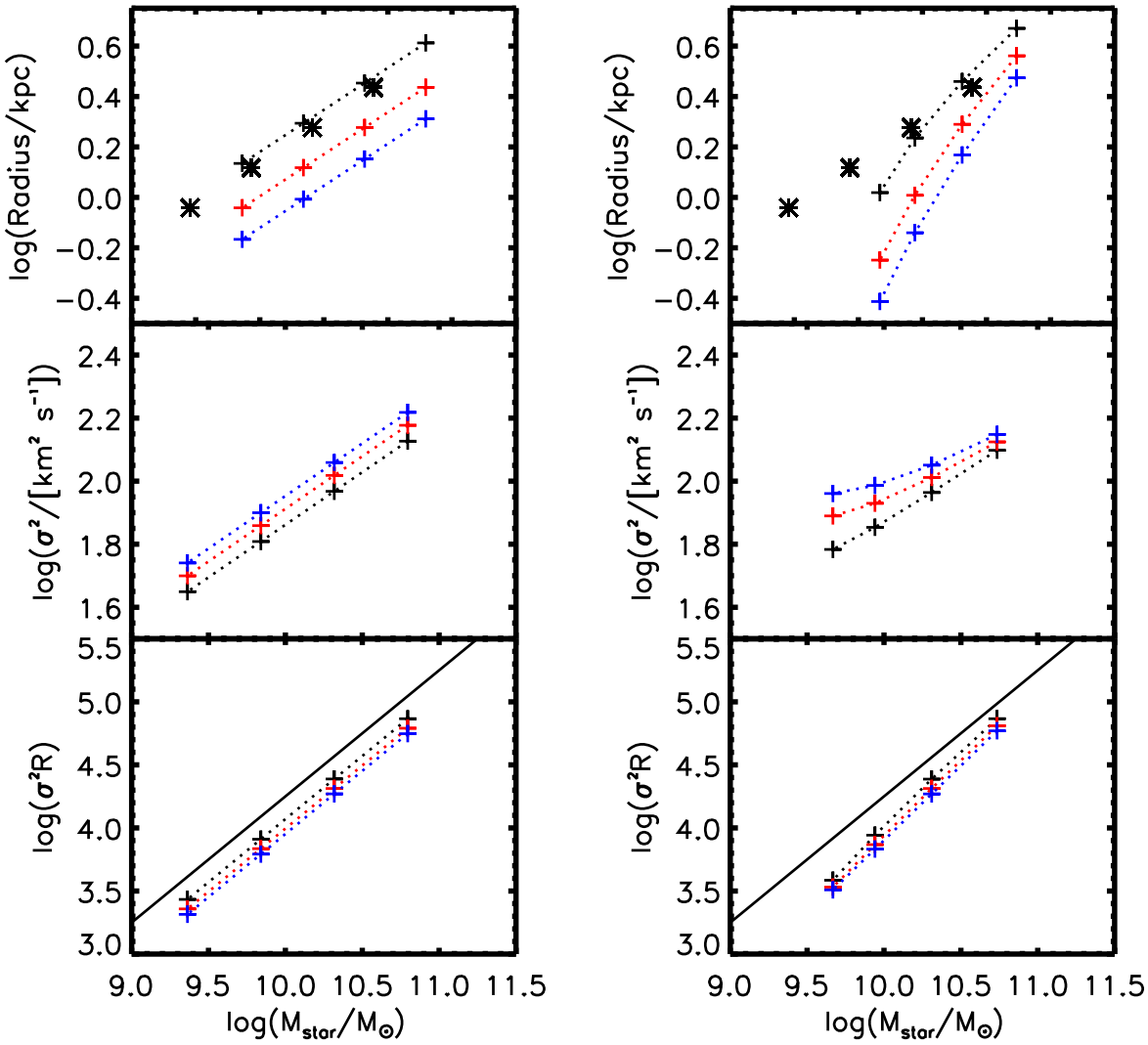

Figure 4. Scaling relations for merger remnants produced by the model from our series of idealized progenitors with a varying radiative energy loss parameter $C_{\rm rad}$, which takes values of 1.0 (black), 3.0 (red), and 5.0 (blue). $C_{\rm rad} = 2.75$ is the calibrated value from the simulations. Dotted lines connect cases with the same value of $C_{\rm rad}$. Progenitors in (a) have a constant gas to stellar mass ratio of 0.5, whereas progenitors in (b) have a changing gas fraction with mass ($\gamma = 0.7$). The top panels show the size-stellar mass relation of the merger remnants (crosses) and progenitors (stars), while the middle and lower panels show the stellar mass FJ relation and the fundamental plane for the merger remnants, respectively. The solid line plotted in the lowest panels shows the FP slope for galaxies with a virial scaling. Changing $C_{\rm rad}$ affects the slopes of the size-mass relation and FJ relation for the cases where gas fraction varies as a function of stellar mass (b), but it does not effect the FP.

tor of ~ 1.5 smaller in radius for a given mass. Dutton et al. (2010) find a similar offset between their re-analysis of SDSS and the results of Shen et al., and argue that this was primarily due to their use of circular rather than elliptical apertures. For this work, we scale the fitting function of Shen et al. to match the normalization of Barden et al. (2005) and Dutton et al. (2010).

For early-type galaxies the median radius is described by

$$\bar{R}(\mathrm{kpc}) = b\left(\frac{M}{\mathrm{M}_\odot}\right)^a, \tag{10}$$

where $a = 0.56$ and $b = 3.47 \times 10^-5$. The scatter in the relation is similar for both late- and early-types with the fit to late-type galaxies being

$$\sigma_{\ln R} = \sigma_2 + \frac{(\sigma_1 - \sigma_2)}{1 + (M/M_0)^2}, \tag{11}$$

where $\sigma_1 = 0.47$ and $\sigma_2 = 0.34$.

The fit for the stellar mass Faber-Jackson relation in SDSS can be found in Gallazzi et al. (2006), and is given by

$$\log(\sigma_v(\mathrm{km\ s^{-1}})) = 0.286 \log(M_*/\mathrm{M}_\odot) - 0.895, \quad (12)$$

where σ_v is velocity dispersion and M_* is the stellar mass. The scatter in the relation is 0.071 dex.

The fundamental plane relation can be represented in a number of projections. However, recent work suggests that the tilt of the plane results from a systematic change in the central dark matter fraction (Zaritsky et al. 2007; Hopkins et al. 2008) as the result of a varying effect of dissipation with mass. A number of observational studies have examined the relationship between central dynamical and stellar mass,

$$M_{\mathrm{dyn}} \propto M_{\mathrm{star}}^{1+\alpha}, \quad (13)$$

and have determined a value of $\alpha \approx 0.2$ (Pahre et al. 1998; Gerhard et al. 2001; Padmanabhan et al. 2004; Gallazzi et al. 2006).

There is little published data on the evolution of the FJ and FP to high redshift**, though observations suggest that any evolution in the FP is minimal up to $z \sim 1$ (Holden et al. 2010; Saglia et al. 2010; Herbert et al. 2011)**. However, a number of studies have examined the evolution of the size-mass relations between $z \sim 0$ and up to $z \sim 3$ (Barden et al. 2005; McIntosh et al. 2005; Trujillo et al. 2006). The most comprehensive of these studies, Trujillo et al. (2006), combines data from SDSS, GEMS (Galaxy Evolution from Morphology and SEDs) and FIRES (Faint Infrared Extragalactic Survey) in order to quantify evolution between $z = 0$ and $z = 3$ for both early- and late-type galaxies. They differentiate galaxies by light concentration according to Sérsic index n and find that for both low-n (late-type) and high-n (early-type) galaxies the mean size at given mass at $z \sim 2.5$ is ~ 2 times smaller than today. Specifically they find that at given stellar mass the sizes of late-type galaxies evolve as $(1+z)^{-0.40\pm0.06}$, whereas the sizes of early-types evolve as $(1+z)^{-0.45\pm0.10}$.

5 COMPARISON WITH OBSERVATIONS

We now apply our merger model to **major mergers of disk-dominated galaxies** from the S08 and Millennium SAMs. These SAMs produce statistical samples of galaxies with properties that are closely matched to those observed in the universe. Thus they provide an effective means for testing the merger model in a cosmological framework. **At every time step in the SAMs, we use the data from all disk-disk major mergers, regardless of the previous or subsequent merger histories of the disks. We emphasize that we are making no attempt to model subsequent evolution or mergers of the elliptical remnants. Possible implications of this further activity are examined in Section 6.** Since the modeled merger remnants are a function of the **disk** progenitor properties, we begin by examining the distributions of galaxy properties in the SAMs and making comparisons to the observed distributions.

5.1 Properties of the Progenitors

In the model, the most important properties of the progenitors are initial size, mass, and gas fraction. Thus we begin by looking at the size-mass distributions of progenitors in each SAM. The relations are plotted for S08 in Figure 5(a) and for Millennium in Figure 5(b). For each figure the progenitors are separated into **one of** six redshift bins **according to the redshift of the merger**. Within each bin, the progenitors are divided into mass bins with a width of 0.2 in $\log(\mathrm{M}_\odot)$. The local relations for low-n (solid blue) and high-n (dotted red) galaxies are shown for comparison. Additionally, the observed redshift evolution of the size of the low-n galaxies (Trujillo et al. 2006) is depicted with the blue-dashed line. This is calculated using the median progenitor redshift in each redshift bin.

The size-mass relation produced by the progenitors in S08 reproduces the observed relation quite nicely, including evolution with redshift. The Millennium progenitors are also fairly close to the observed relation, but in the lowest redshift bin they are $\sim 50\%$ too large on average. This gap lessens with increasing redshift. Also of note is that the highest mass bin is typically systematically high. It is also interesting to note the difference in slope between the observed size-mass relations for early- and late-type galaxies. As noted before, if a merger explanation of the elliptical size-mass relation is to be successful, it must explain the rotation between the two observed relations. We discuss this with respect to our model in the next section.

Observing cold gas within galaxies is extremely challenging. However a study by Kannappan (2004) used a photometric estimate of gas fraction in order to calculate the changing ratio of gas to stellar mass (G/S) with galaxies from SDSS. Calura et al. (2007) use star formation rates from a large SDSS sample combined with theoretical modeling to estimate (G/S) as a function of both stellar mass and redshift. Neither study provides fits to the observed relation, but it can be seen from Figure 5 of Calura et al. (2007) that, for $z < 0.1$,

$$\log(G/S) \sim -0.5 \log(M/\mathrm{M}_\odot) + C, \quad (14)$$

where for blue galaxies $C \sim 4.6$ and for red galaxies $C \sim 4.1$. The values of $\log(G/S)$ falls approximately in a range between -4 and 1.5.

The relation between G/S and stellar mass in the SAMs is shown in Figures 6(a) and 6(b). The observational relation (Equation 14) is also depicted to show that the progenitors from the SAMs have gas fraction to stellar mass relations with slopes similar to those observed. However, the distribution of progenitor gas fractions from the SAMs is not expected to exactly align with the depicted observed relations for two reasons: 1) even the lowest redshift bin ($0 < z < 0.3$) from the SAMs includes redshifts significantly higher than those from the observations ($z < 0.1$), and 2) the progenitors are a small subset of all galaxies. Specifically, the galaxies shown from the SAMs are those that undergo major mergers during the specified redshift and are disk-dominated. The properties of this subset may differ from both the red and blue populations in the observations. In fact, the models of S08 have been tuned to reproduce the gas fraction vs. stellar mass observations of Kannappan (2004) for spirals.

It can be seen that the distributions of G/S in both

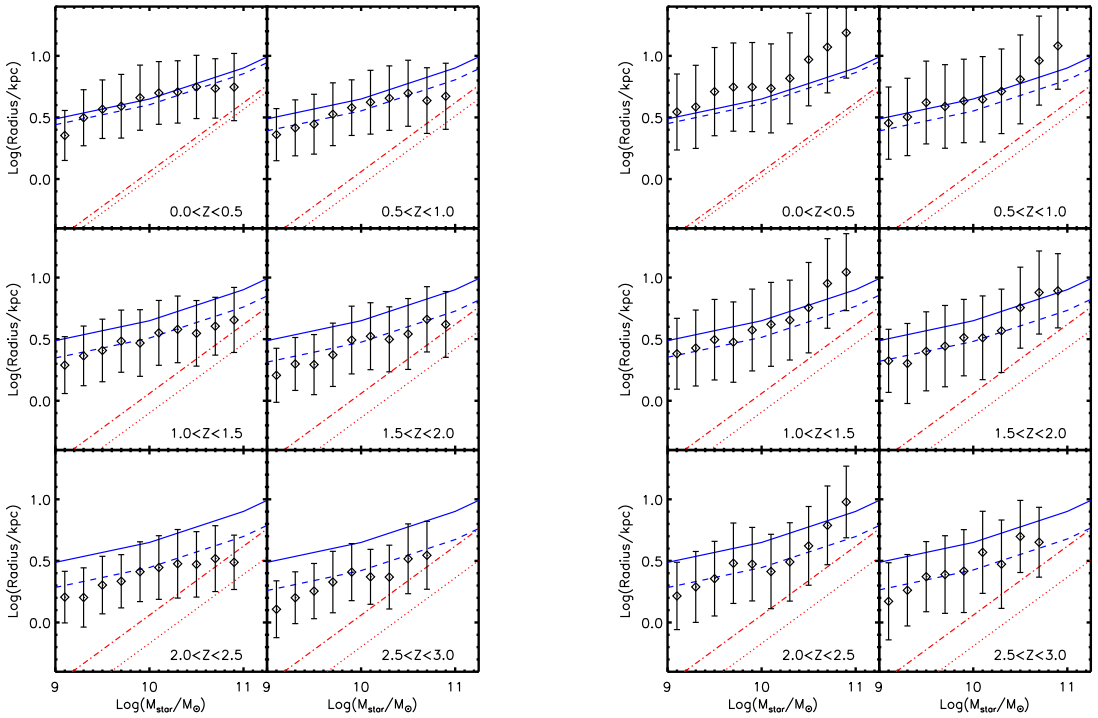

(a) (b)

Figure 5. Size Mass relations for the progenitors in the S08 SAM (a) and the Millennium SAM, binned by redshift. Symbols denote the median of the progenitor distribution in the SAM, and error bars depict the 1σ spread in the distribution. The solid (blue) line and the dashed (red) line depict the redshift zero relations from Shen et al. (2003) of the low-n and high-n populations respectively. The blue-dashed and red-dotted lines depict the evolution of the low-n and high-n relations respectively with redshift as given by Trujillo et al. (2006). This is calculated using the median redshift for the progenitors in each bin. For this and subsequent scaling relations figures, blue and red lines denote observed scaling relations of disk and elliptical galaxies respectively.

SAMs are bimodal with a gas-rich (blue) and gas-poor (red) sequence. While both SAMs capture the slope of the observed relation, they have gas to baryonic mass power law slopes which are significantly less than the $\gamma = 0.7$ value suggested in Dekel & Cox (2006) and the idealized mergers presented above. A majority of the mergers are gas-rich; 99% and 92% of all mergers, for S08 and Millennium respectively, have total progenitor gas fractions greater than 0.1. The relation from the SAMs only evolves very modestly over time, but for both SAMs the fraction of mergers that are coming from high gas fraction progenitors increases with increasing redshift. This is seen both as a disappearance of the red sequence (in S08) and a decrease in the typical mass of progenitors as redshift increases (both SAMs). **A recent study (Tacconi et al. 2010) found that the gas fraction of star-forming galaxies increases by a factor of a few as the redshift increases from $z = 0$ to $z \sim 2.3$. While we have made no selection cuts to ensure that our spiral progenitors are star-forming, these results suggest that the gas fractions of major mergers might increase over time.**

There are also interesting correlations between gas fraction and size. To demonstrate this, we replot the size-mass relation with points drawn for progenitors colored by G/S (see Figures 7(a) and 7(b)). Red points are gas-poor with $-2.0 < \log(G/S) < -1.0$. Green points have intermediate gas fractions with $-1.0 < \log(G/S) < 0.0$. Blue points are gas rich with $0.0 < \log(G/S) < 1.0$. For both SAMs, at given mass there is a significant trend of gas fraction with size: *the larger radius progenitors have higher gas fractions.* This is because these galaxies have lower densities and therefore have lower star formation rates and have consumed less of their gas, since both SAMs assume a Kennicutt-Schmidt-type relationship for star formation (star formation rate density is proportional to a power of the gas density). **A similar trend has been observed in a study of nearby galaxies (Catinella et al. 2010).** This has important implications for the evolution of scaling relations via merging. Remember that dry merging moves galaxies up and to the right on the plot, that is, it increases both mass and size (Figure 2(a)). Because of their location far above the late-type scaling relation, dry merging would not take the larger radius progenitors on to the desired relation for remnants. However, since these galaxies are gas-rich they can travel with a horizontal or even somewhat downward vector when they merge. Additionally, this convergence of merging vectors within a single mass bin, such that the gas-poor compact galaxies move to larger radii while the gas-rich low

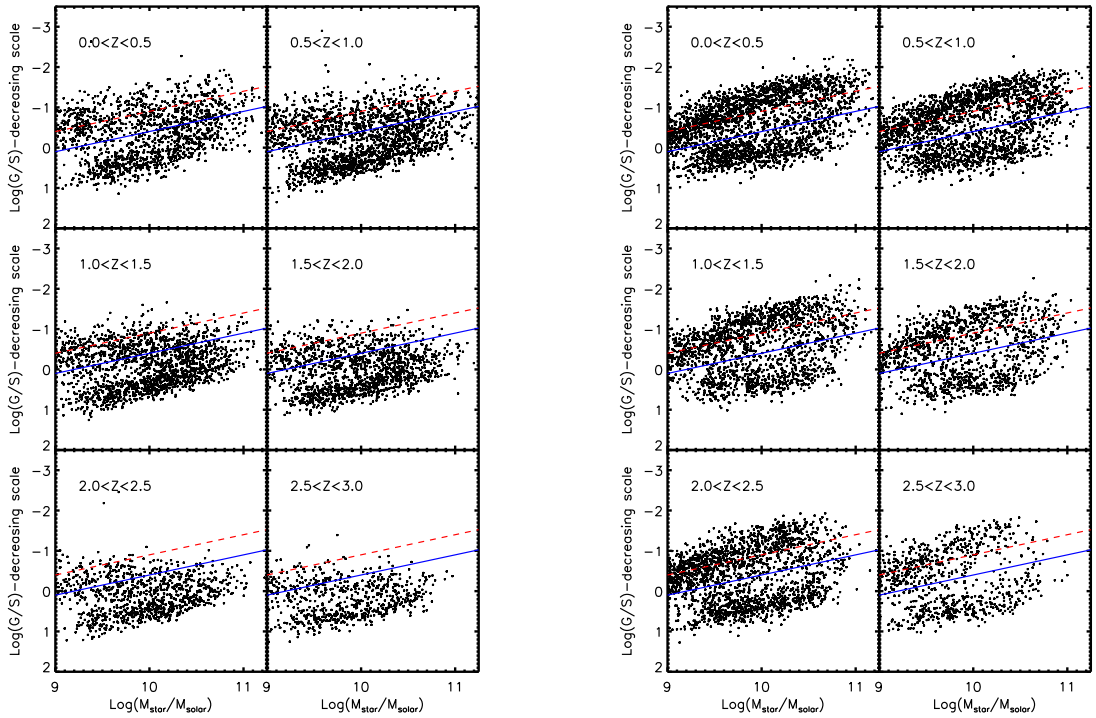

(a) (b)

Figure 6. The relation between G/S and stellar mass for the progenitors in the S08 SAM (a) and the Millennium SAM (b). Points are galaxies from the SAM. The blue (solid) and red (dashed) lines are approximate fits to observations of nearby galaxies in the SDSS (Kannappan 2004; Calura et al. 2007), with blue representing the relation for blue galaxies and red for red galaxies. $\log(G/S)$ is plotted using a decreasing scale as in the observational studies. The observed relations and SAM progenitors display similar slopes, but the relations are not expected to exactly coincide due to differences in redshift ranges and selection effects.

density galaxies move to smaller radii, results in a reduction of scatter for the remnant scaling relations. *This effect may contribute to the small scatter in the observed early-type size-mass relation.*

5.2 Properties of the Merger Remnants

Given progenitor properties, the merger model allows us to predict the sizes, stellar masses, and velocity dispersions of the merger remnants. We now exploit this ability to explore the buildup and evolution of the remnant scaling relations as predicted by the models. In this subsection we use the simplified merger model described in Section 2. For comparison we will show results on the size-mass relation using the more elaborate C08 model and summing over merger orbits in subsection 5.3 below.

The remnant size-mass relation for the SAMs is shown in Figures 8(a) and 8(b). Note that we are comparing the size-mass relations for *all* observed early-type galaxies at a given epoch with that for just the remnants of disk major mergers that occurred in that redshift bin. This neglects early-types that formed at earlier epochs, and have not had a recent merger, as well as early-types formed by mixed-morphology mergers. In addition, we only model binary mergers, and do not account for multiple mergers **or subsequent evolution following the formation event**. Therefore, this may not be a fair comparison, but it is the best we can do until we implement the merger model within SAMs.

The model applied to the S08 SAM overpredicts the typical observed sizes for a given mass by about 0.3 dex at low masses, and the slope is steeper than observed. However, the S08 results roughly capture the magnitude of observed evolution in average sizes from smaller sizes at high redshift to larger sizes at low redshift (see also Trujillo et al. 2006; Trujillo et al. 2007; Franx et al. 2008). The slope of the size-mass relation is slightly shallower than the observed slope at all redshifts, but the merger model has produced a significant steepening from the progenitor size-mass relation as a result of the mass dependent gas fraction in the progenitors.

The average predicted size for early-type galaxies in the Millennium SAM is too large, sometimes by more than 0.5 dex. Millennium produces a different normalization for the size-mass relation than S08 for two reasons: 1) the progenitors are larger, and 2) the progenitors have less gas. The slope of the relation is also much shallower than observed. This is likely the result of differences in progenitor gas fractions between the two SAMs. The evolution in the Millennium size-mass relationship is such that in the highest redshift bin ($2.5 < z < 3.0$) the average size at a given mass

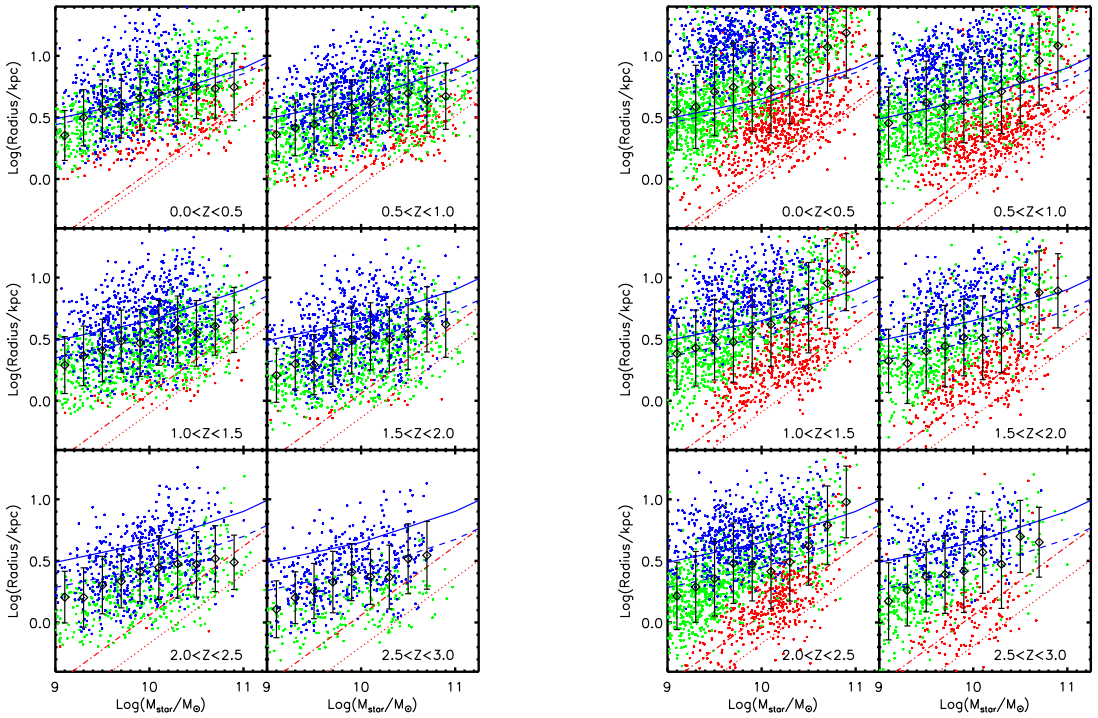

(a) (b)

Figure 7. Size-Mass relations for the progenitors in the S08 SAM (a) and Millennium SAM (b), binned by redshift and including points for progenitors colored by gas fraction. Red denotes $-2.0 < \log(G/S) < -1.0$. Green denotes $-1.0 < \log(G/S) < 0.0$. Blue denotes $0.0 < \log(G/S) < 1.0$. Other symbols and lines are as in Figure 5(a). Both SAMs produce systematic gradients in disk galaxy gas fractions as a function of size at given mass. This results from higher star formation rates, and therefore faster gas consumption in denser galaxies. When dissipative effects are included in a merger model, these systematic gradients result in smaller scatter in the merger remnant size-mass relation.

is ~ 3 times smaller than in the lowest redshift bin. This is within the errors on the observed evolution.

In addition to sizes, the merger model predicts values for velocity dispersion (σ), so we also examine the stellar-mass Faber-Jackson relation (FJ) (see Figures 9(a) and 9(b)). The S08 model roughly produces the correct slope for the local FJ relation. However, Millennium produces a slightly steeper slope than observed in most redshift bins, particularly at high mass. S08 slightly underpredicts (~ 0.05 dex) velocity dispersions at $z = 0$, whereas the offset for the Millennium relation is larger (~ 0.2 dex). Since remnants from Millennium are systematically too large, they also have systematically low velocity dispersions. Both SAMs show an evolution of the FJ relation with redshift. Within the model there are two possible mechanisms for evolution in σ at a given mass: evolving size and evolving dark matter halo properties. For S08 σ at a given mass increases by roughly a factor of 1.4 between $z = 0$ and $z = 3$; for Millennium σ increases by a factor of two. These values are commensurate with the decrease in size at a given mass for S08 and Millennium, suggesting that changing dark matter properties have little effect on the evolution. It is not known yet whether this evolution is consistent with the real universe.

Finally, we examine the fundamental plane (FP) relation predicted by the merger model. The model uses the virial relation to predict values for σ, however the mass used in the model is a dynamical mass that includes a contribution from dark matter. Therefore, if a tilt is produced by the model in the virial projection of the FP, then it is purely a result of changing dark matter content in the galaxy centers. In Figures 10(a) and 10(b) we plot the relation between $\sigma^2 r \propto M_{\rm dyn}$ and stellar mass. The merger model applied to the S08 progenitors does not reproduce the observed tilt in the FP, with slopes roughly the same as would be expected from the virial relation. For Millennium the FP is tilted in the same sense as is suggested by observations, with dynamical mass increasing faster than stellar mass, and the tilt produced is only slightly less than observed. This tilt results from the contrasting dissipational and dissipationless evolution of the baryonic and dark matter components combined with the gas gradient in the progenitors. Lower mass progenitors have higher gas fractions and therefore produce more compact stellar remnants with smaller central dark matter fractions. Higher mass progenitors have smaller gas fractions and therefore end up with a sparser stellar center, resulting in larger central dark matter fractions.

Plotting σ versus r gives a nearly face-on view of the FP, and allows us to determine the portion of the FP be-

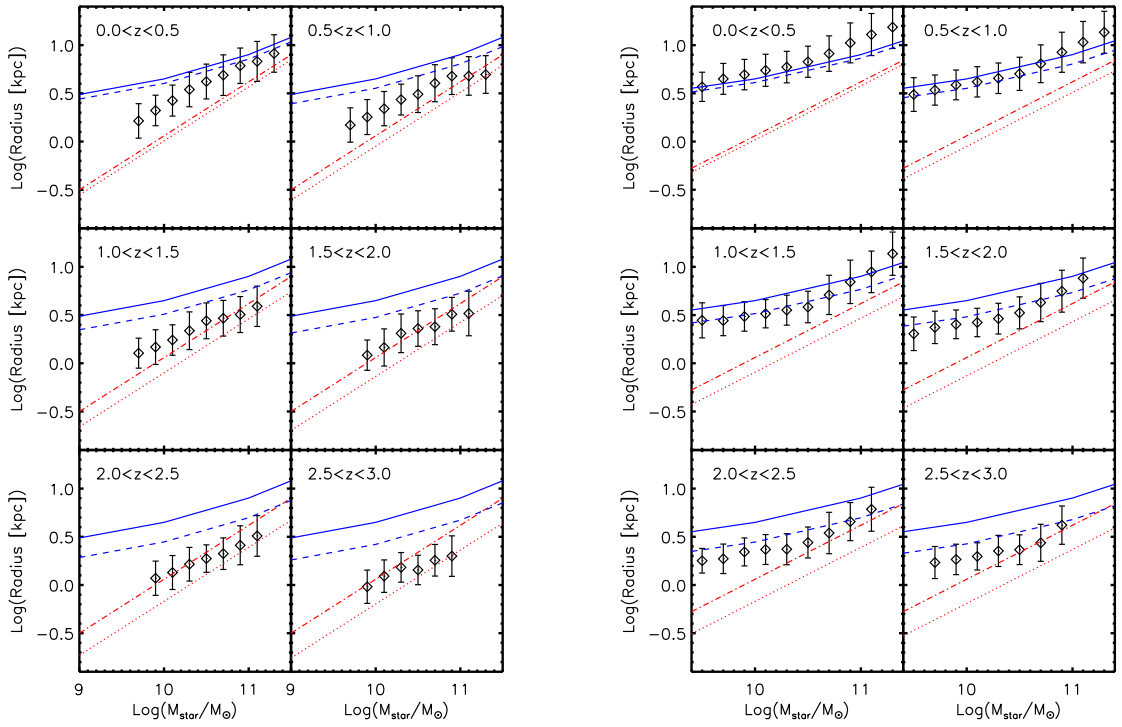

(a) (b)

Figure 8. Size-Mass relations for the remnants in the S08 SAM (a) and Millennium SAM (b), binned by redshift. Lines are observed relations as in Figure 5(a). The S08 SAM captures most of the steepening that occurs between the observed late- and early-type scaling relations, whereas the slope produced by the Millennium SAM remains near that of the progenitors (disks). Both SAMs show roughly the right amount of evolution in size between z=3 and z=0, but both also overpredict the sizes for a given mass.

ing populated at a given redshift by major mergers of disk galaxies. We show this relationship for both S08 (Figure 11(a)) and Millennium (Figure 11(b)). Both SAMs show a correlation between σ and r such that galaxies with larger sizes also tend to have larger velocity dispersions. This is similar to a correlation observed at low redshift in the SDSS (Graves et al. 2009). Most interesting perhaps is the noticeable evolution with redshift across the face of the FP. At high redshift the mergers produce primarily high σ galaxies with relatively small sizes. As time progresses toward $z = 0$, the typical σ of a merger remnant decreases and the typical size increases, as the correlation between the size and velocity dispersion marches across the face of the plane. Graves et al. (2009) also see this correlation between σ and age, but not between size and age. Also, at any given redshift there is a stronger correlation between σ and r in our model than seen in SDSS. However, as discussed earlier, in reality each bin would also contain remnants that were formed at earlier times, which would weaken the correlation. Furthermore, one would expect that the remnants from higher redshifts would be modified by further merging, which could also increase the radius and scatter across the plane. An interesting question that remains unanswered is whether there are specific regions of the FP space that are not populated by major merging. We are working on further studies of the age and metallicity predicted by our merging model implemented self-consistently within the SAMs, and will report the results in a forthcoming paper (Porter et al. in prep).

5.3 Scaling relations produced with the C08 Model

The new simplified merger model described above captures much of the behavior of the C08 model. However, when applied to the SAMs, the results of the two models are not identical. To illustrate the differences, we show the scaling relations produced using the C08 model (Figures 12, 13, and 14). Aside from using the new, extended model for central dark matter fraction (Appendix A), the model is implemented as described in C08. For both SAMs the C08 model results in a more pronounced steepening of the size-mass relation. In fact, at low redshift, for S08 the relation produced has a slope that is too steep, whereas for Millennium the slope is close to that observed. Of the three scaling relations, the size-mass relation is the one that shows the largest difference between the two models. However, C08 also produces a stronger tilt in the FP relation for both SAMs, with both SAMs having a tilt that is close to that observed. Though we believe these differences arise from variations in the gas fractions and concentrations of the progenitors, we will refrain from a more detailed comparison until the models are directly implemented within the SAMs.

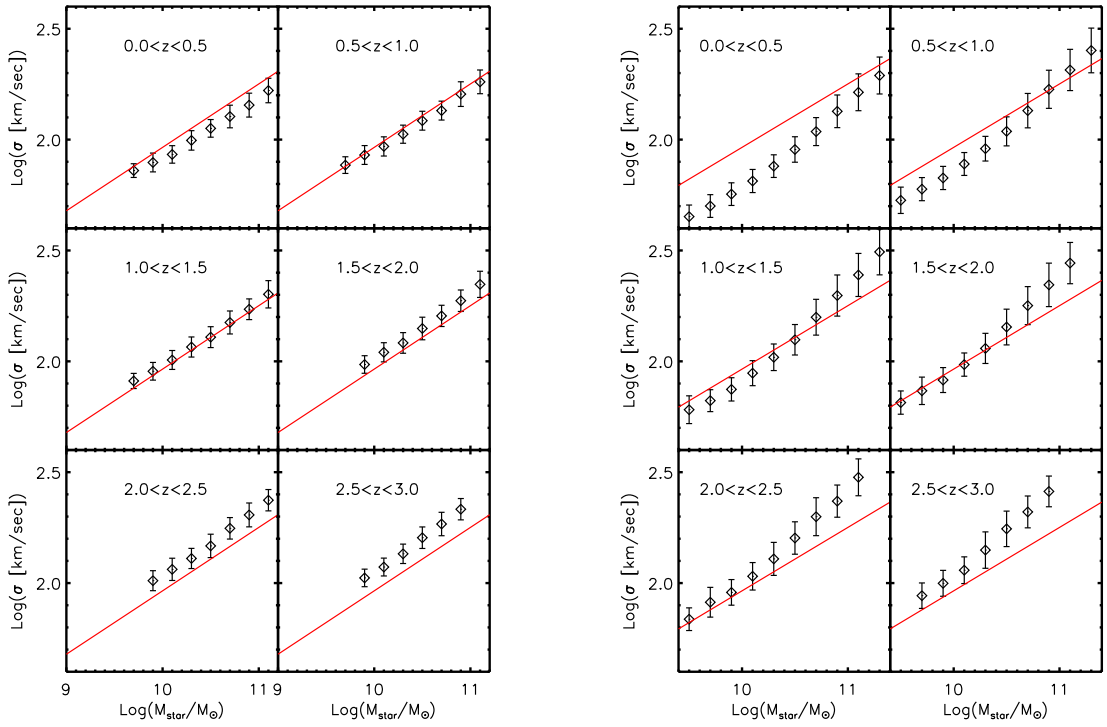

(a) (b)

Figure 9. Faber-Jackson relations for the remnants in the S08 SAM (a) and Millennium SAM (b), binned by redshift. The red line is the observed relation at low redshift (Gallazzi et al. 2006). The S08 SAM produces the correct slope for the FJ relation, whereas the Millennium SAM relation is somewhat steeper than observed. Both SAMs also underpredict velocity dispersions for a given mass at z=0, though the problem is much more severe with the Millennium SAM. Both SAMs show evolution in the normalization of the FJ relation since z=3. This is not yet constrained by observations.

6 DISCUSSION

A continuing question in the field of galaxy formation is the role that mergers play in constructing elliptical galaxies. Shen et al. (2003) have suggested that it is difficult to get the proper elliptical size-mass relation from repeated major mergers of disk galaxies because of the rotation between the early- and late-type relations. Recent SAMs confirm this result, and also produce a scatter in the remnant size-mass relation that is much too large (Shankar et al. 2010; Guo et al. 2010). However, these models do not take into account the effects of dissipation and a possible dependence of gas fraction on progenitor mass, **as has been done in several high-resolution hydrodynamical simulations (Dekel & Cox 2006; Robertson et al. 2006; Hopkins et al. 2008)**. Here we demonstrate that if the effect of dissipation is included **within SAMs** and if the progenitors have a decreasing gas fraction with increasing mass, then this results in a steeper size-mass relation for the merger remnants **compared to the disk progenitors**. Furthermore, since less dense disks have lower star formation rates, the disk galaxy progenitors have increasing gas fractions with increasing size at a given mass. Applying a dissipative merger model to progenitors with this trend in gas fraction also reduces the scatter in the size-mass relation, as explained at the end of Section 5.1. In fact, our model, with a typical dispersion of 0.2 dex in the size-mass relation, has less than the 0.3-0.4 dex dispersion in the relation observed by Shen et al. (2003). That our dispersion is too small might be expected, since we are only considering major mergers of disk galaxies, a subset of the total early-type population. **As noted above, we are also separating the size-mass relation according to the redshift of the merger. In order to directly compare to observations, we would need to include all the mergers that have occurred at any given redshift.** Comparison of the progenitor and remnant properties suggests that the overall normalization of the early-type size-mass relation is determined by a combination of the size-mass relation of the progenitor disk galaxies and the normalization of the gas fraction relation.

In order to capture the observed Faber-Jackson (FJ) relation, it is necessary to track the changing central dark matter fraction. The results from our model suggest that the FJ relation may evolve modestly over time such that early-type galaxies at a given mass have larger velocity dispersions at higher redshift. The merger model applied to progenitors from the S08 SAM results in a slope close to the virial slope, which is slightly shallower than the observed slope. The model applied to progenitors from the Millen-

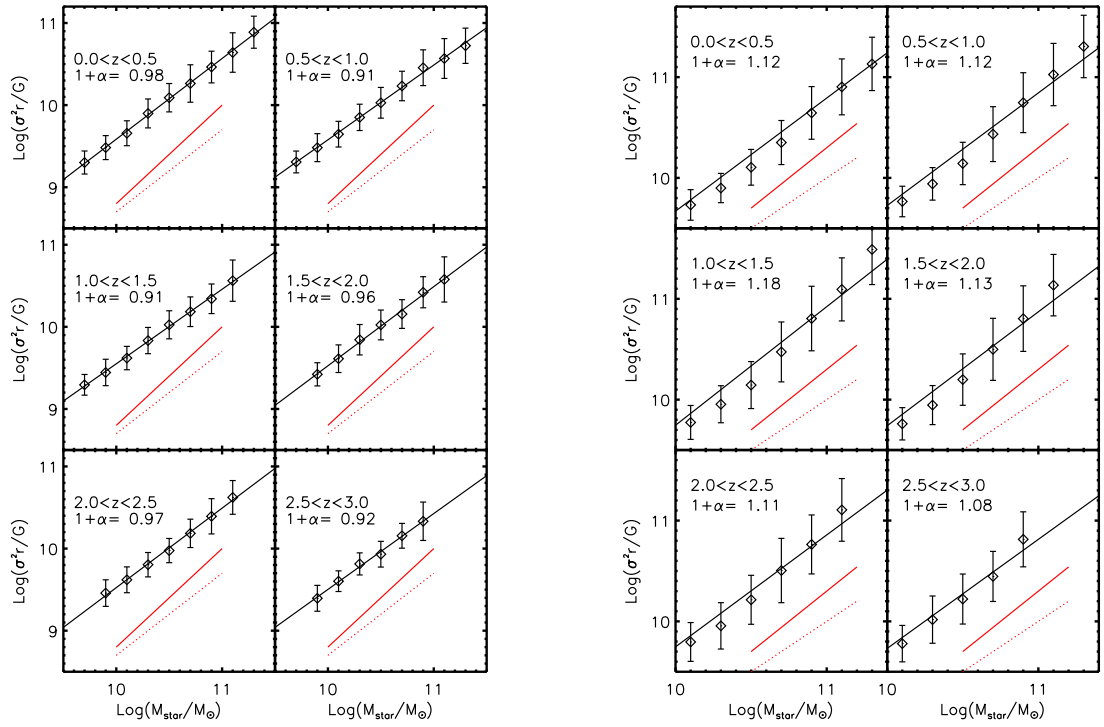

(a) (b)

Figure 10. Fundamental plane plotted as $M_{\rm star}$ versus M_{dyn} for the remnants in the S08 SAM (a) and Millennium SAM (b), binned by redshift. The solid red line shows the observed scaling of $M_{\rm dyn} \propto M_{\rm star}^{1.2}$, and the dotted red line shows the virial scaling. The black line is a fit to the SAM remnants with $M_{\rm dyn} \propto M_{\rm star}^{1+\alpha}$ and $1+\alpha$ is shown on the figure. Neither SAM completely captures the observed tilt of the FP. S08 produces tilts that are somewhat less than virial, while Millennium is much closer to the observed tilt with $1+\alpha = 1.12$ at z=0.

nium SAM reproduces the observed tilt in the fundamental plane (FP), but this agreement appears to be a fortuitous cancellation between sizes that are too large and velocity dispersions that are too small at a given mass. The tilt predicted by the model is the result of a changing central dark matter fraction with mass that results from a mass dependence of gas fractions in the progenitors. Higher mass progenitors have less gas and therefore less dissipation during their mergers, resulting in remnants with a less concentrated stellar center and consequently a higher dark matter fraction. In the face-on view of the FP, the remnants evolve from higher σ and lower r at high redshift to lower σ and higher r at low redshift.

It is important to note that, since we calculate remnant properties during post-processing, the scaling relations derived using the model in this paper do not capture the entire elliptical population at each redshift. Rather they depict the scaling relations of elliptical galaxies being added to the population via major mergers of disks at a given redshift. One would expect that the high-redshift galaxies would undergo further accretion and merging, including minor merging and dry merging in some cases **(see e.g. Bezanson et al. 2009; Oser et al. 2010). In particular, minor mergers between a large, gas-poor elliptical and several small spirals have been shown to greatly increase the effective radius of the elliptical while leaving the velocity dispersion nearly unchanged (Naab et al. 2009).** Moreover some early-type galaxies may be formed via mergers involving one or more early-type progenitors, which are also neglected here. We find that approximately one-third of the low-redshift spheroids at all masses are accounted for by disk-disk major mergers, so it could be misleading to compare our model outputs with all observed early-type galaxies at various redshifts.

We also note that there are differences between the results of the simple model used here and the previous model of C08. Without fully implementing the models within the SAMs and tuning the various model parameters, it is difficult to know which model will ultimately produce more favorable results. The simple model requires fewer unknown parameters, and therefore is preferred if it produces reasonable results. However, *the key conclusions of this work are that the steepening* **and reduced scatter of the size-mass relation from that of disk galaxies**, *and the tilt in the fundamental plane can all be produced by accounting for dissipation during galaxy mergers.* While the strength of these effects will vary by model, the effects themselves are expected to be general features of any realistic merger model that accounts for dissipation.

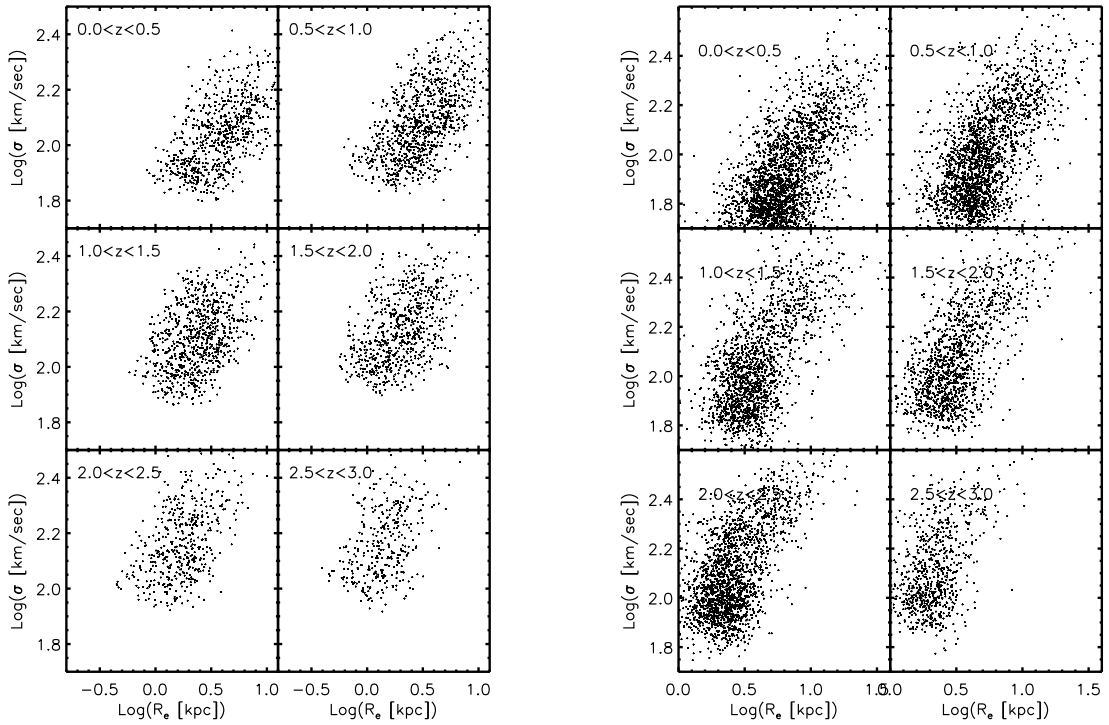

(a) (b)

Figure 11. Nearly face-on view of the fundamental plane plotted as r versus σ for the remnants in the S08 SAM (a) and Millennium SAM (b), binned by redshift. Both SAMS show some positive correlation between velocity dispersion and size at all redshifts. From z=3 to z=0 remnants also gradually migrate from higher dispersion and smaller size to lower dispersion and larger size.

In future work, it will be useful to a incorporate a dissipational merger model within semi-analytic models. This will allow a more comprehensive exploration of the evolution of galaxy scaling relations via merging by allowing the inclusion of a wider variety of progenitor types, and enable the study of correlations with other quantities such as age and metallicity. However, even the simple external processing of SAM progenitors as carried out in this study shows that mergers are a viable mechanism for the production of a large fraction of elliptical galaxies. Furthermore, we find that the elliptical scaling relations are plausibly explained given the combination of progenitor scaling relations and gas fractions.

Acknowledgments

MC, AD, and JRP acknowledge support from NASA ATP grant NNX07AG94G and NSF grant 1010033 at UCSC. DC acknowledges receipt of a QEII Fellowship awarded by the Australian government. The work of AD was partly supported by ISF grant 6/08, by GIF grant G-1052-104.7/2009, and by a DIP grant. We also thank T. J. Cox, Sandra Faber, Jenny Graves, Patrik Jonsson, and Thorsten Naab for helpful conversations. Finally, we thank the anonymous referee for many suggestions and questions that helped us to clarify the paper.

REFERENCES

Barden M., Rix H.-W., Somerville R. S., Bell E. F., Häußler B., Peng C. Y., Borch A., Beckwith S. V. W., Caldwell J. A. R., Heymans C., Jahnke K., Jogee S., McIntosh D. H., Meisenheimer K., Sánchez S. F., Wisotzki L., Wolf C., 2005, ApJ, 635, 959

Barnes J. E., Hernquist L., 1992, ARA&A, 30, 705

Barnes J. E., Hernquist L., 1996, ApJ, 471, 115

Benson A. J., 2005, MNRAS, 358, 551

Benson A. J., 2010, ArXiv e-prints

Benson A. J., Bower R., 2010, MNRAS, 405, 1573

Bernardi M., Sheth R. K., Annis J., Burles S., Eisenstein D. J., Finkbeiner D. P., Hogg D. W., Lupton R. H., Schlegel D. J., SubbaRao M., York D. G., 2003a, AJ, 125, 1849

Bernardi M., Sheth R. K., Annis J., Burles S., Eisenstein D. J., Finkbeiner D. P., Hogg D. W., Lupton R. H., Schlegel D. J., SubbaRao M., York D. G., 2003b, AJ, 125, 1866

Bezanson R., van Dokkum P. G., Tal T., Marchesini D., Kriek M., Franx M., Coppi P., 2009, ApJ, 697, 1290

Bolton A. S., Burles S., Treu T., Koopmans L. V. E., Moustakas L. A., 2007, ApJL, 665, L105

Bolton A. S., Treu T., Koopmans L. V. E., Gavazzi R., Moustakas L. A., Burles S., Schlegel D. J., Wayth R., 2008, ArXiv e-prints, 805

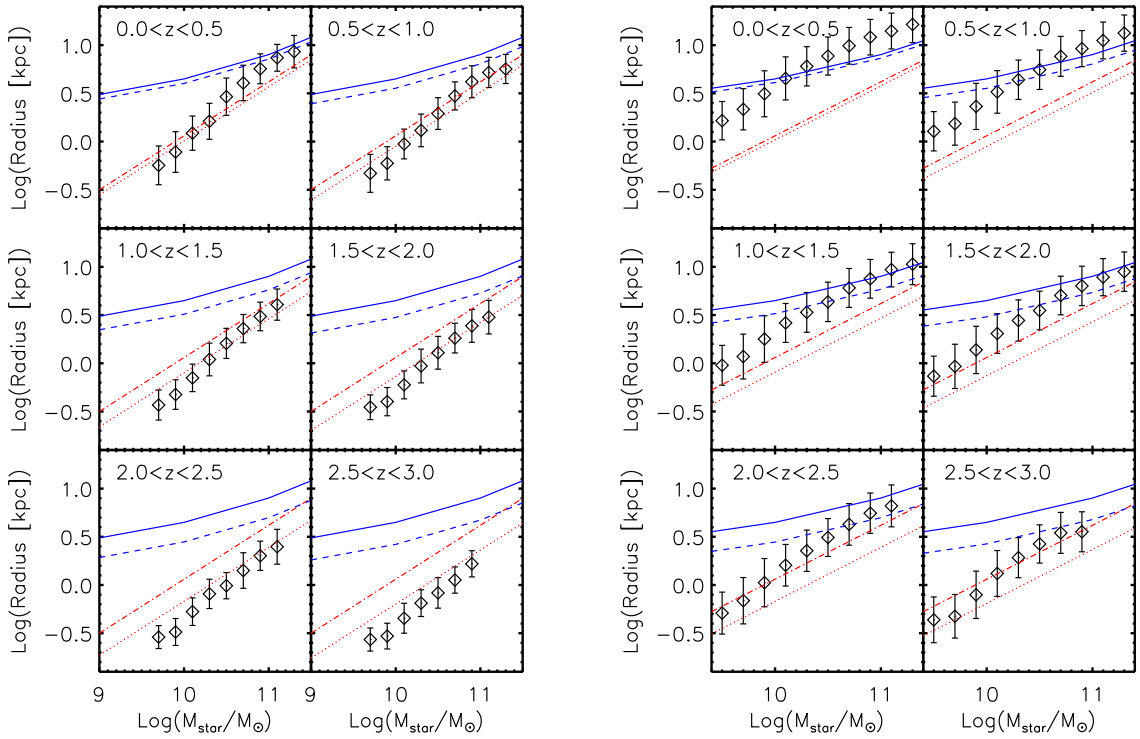

(a) (b)

Figure 12. Size mass relations produced by the C08 model combined with the new model for central dark matter fractions, applied to S08 (a) and Millennium (b). For both SAMs the relation is steeper than that produced by the simpler model.

Bournaud F., Chapon D., Teyssier R., Powell L. C., Elmegreen B. G., Elmegreen D. M., Duc P.-A., Contini T., Epinat B., Shapiro K. L., 2011, ApJ, 730, 4

Bournaud F., Jog C. J., Combes F., 2007, A&A, 476, 1179

Bournaud F., Powell L. C., Chapon D., Teyssier R., 2010, ArXiv e-prints, 1012, 5227

Bower R. G., Benson A. J., Malbon R., Helly J. C., Frenk C. S., Baugh C. M., Cole S., Lacey C. G., 2006, MNRAS, 370, 645

Bryan G. L., Norman M. L., 1998, ApJ, 495, 80

Buitrago F., Trujillo I., Conselice C. J., Bouwens R. J., Dickinson M., Yan H., 2008, ApJL, 687, L61

Calura F., Jimenez R., Panter B., Matteucci F., Heavens A. F., 2007, ArXiv e-prints, 707

Cappellari M., Bacon R., Bureau M., Damen M. C., Davies R. L., de Zeeuw P. T., Emsellem E., Falcón-Barroso J., Krajnović D., Kuntschner H., McDermid R. M., Peletier R. F., Sarzi M., van den Bosch R. C. E., van de Ven G., 2006, MNRAS, 366, 1126

Catinella et al. 2010, MNRAS, 403, 683

Cimatti A., Cassata P., Pozzetti L., Kurk J., Mignoli M., Renzini A., Daddi E., Bolzonella M., Brusa M., Rodighiero G., Dickinson M., Franceschini A., Zamorani G., Berta S., Rosati P., Halliday C., 2008, A&A, 482, 21

Ciotti L., Lanzoni B., Volonteri M., 2007, ApJ, 658, 65

Cole S., Aragon-Salamanca A., Frenk C. S., Navarro J. F., Zepf S. E., 1994, MNRAS, 271, 781

Cole S., Lacey C. G., Baugh C. M., Frenk C. S., 2000, MNRAS, 319, 168

Cook M., Barausse E., Evoli C., Lapi A., Granato G. L., 2010, MNRAS, 402, 2113

Covington M., Dekel A., Cox T. J., Jonsson P., Primack J. R., 2008, MNRAS, 384, 94

Covington M. D., 2008, PhD thesis, University of California, Santa Cruz

Cox T. J., 2004, PhD thesis, UC Santa Cruz

Cox T. J., Jonsson P., Primack J. R., Somerville R. S., 2006, MNRAS, 373, 1013

Cox T. J., Jonsson P., Somerville R. S., Primack J. R., Dekel A., 2008, MNRAS, 384, 386

Croton D. J., Springel V., White S. D. M., De Lucia G., Frenk C. S., Gao L., Jenkins A., Kauffmann G., Navarro J. F., Yoshida N., 2006, MNRAS, 365, 11

De Lucia G., Springel V., White S. D. M., Croton D., Kauffmann G., 2006, MNRAS, 366, 499

Dekel A., Cox T. J., 2006, MNRAS, 370, 1445

Djorgovski S., Davis M., 1987, ApJ, 313, 59

Dressler A., Lynden-Bell D., Burstein D., Davies R. L., Faber S. M., Terlevich R., Wegner G., 1987, ApJ, 313, 42

Dutton A. A., van den Bosch F. C., Faber S. M., Simard L., Kassin S. A., Koo D. C., Bundy K., Huang J., Weiner B. J., Cooper M. C., Newman J. A., Mozena M., Koekemoer A., 2010, ArXiv e-prints

Faber S. M., Jackson R. E., 1976, ApJ, 204, 668

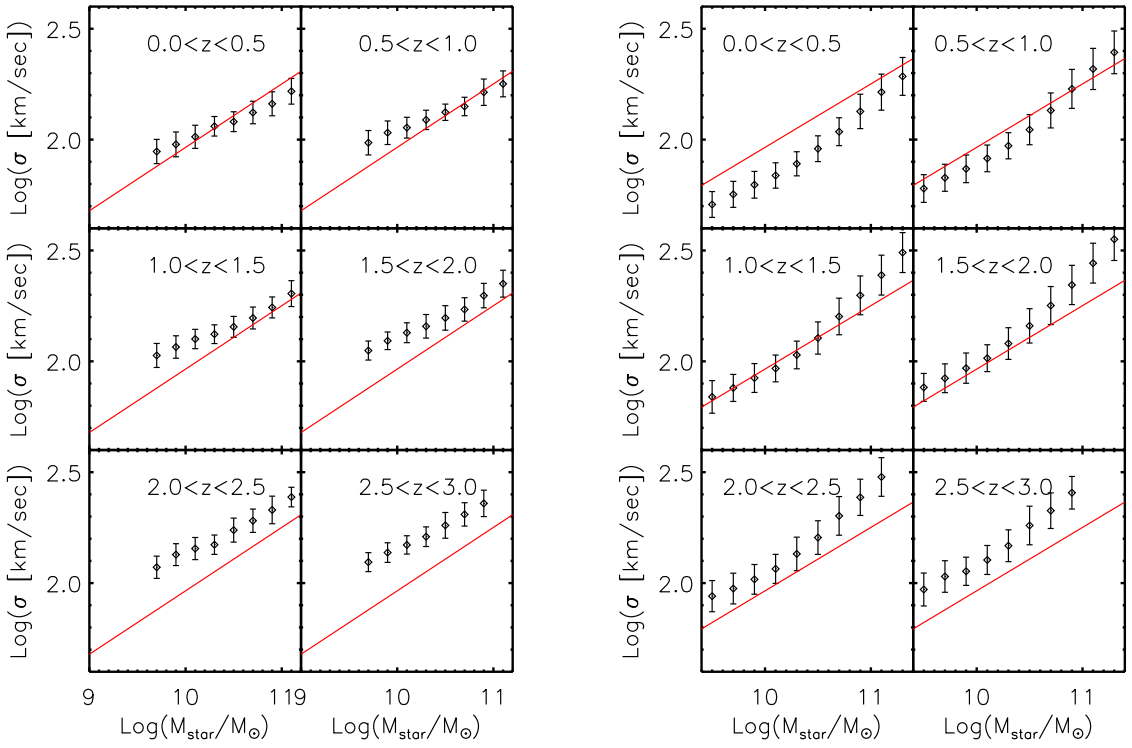

Figure 13. The Faber-Jackson relations produced by the C08 model combined with the new model for central dark matter fractions, applied to S08 (a) and Millennium (b).

Fan L., Lapi A., Bressan A., Bernardi M., De Zotti G., Danese L., 2010, ApJ, 718, 1460

Fontanot F., De Lucia G., Monaco P., Somerville R. S., Santini P., 2009, MNRAS, 397, 1776

Franx M., van Dokkum P. G., Schreiber N. M. F., Wuyts S., Labbé I., Toft S., 2008, ApJ, 688, 770

Gallazzi A., Charlot S., Brinchmann J., White S. D. M., 2006, MNRAS, 370, 1106

Gerhard O., Kronawitter A., Saglia R. P., Bender R., 2001, AJ, 121, 1936

Graves G. J., Faber S. M., Schiavon R. P., 2009, ApJ, 698, 1590

Guo Q., White S., Boylan-Kolchin M., De Lucia G., Kauffmann G., Lemson G., Li C., Springel V., Weinmann S., 2010, ArXiv e-prints

Hatton S., Devriendt J. E. G., Ninin S., Bouchet F. R., Guiderdoni B., Vibert D., 2003, MNRAS, 343, 75

Herbert P. D., Jarvis M. J., Willott C. J., McLure R. J., Mitchell E., Rawlings S., Hill G. J., Dunlop J. S., 2011, MNRAS, 410, 1360

Holden B. P., van der Wel A., Kelson D. D., Franx M., Illingworth G. D., 2010, ArXiv e-prints, 1009, 4479

Hopkins P. F., Cox T. J., Hernquist L., 2008, ArXiv e-prints, 806

Hopkins P. F., Cox T. J., Younger J. D., Hernquist L., 2009, ApJ, 691, 1168

Kannappan S. J., 2004, ApJL, 611, L89

Kauffmann G., White S. D. M., Guiderdoni B., 1993, MNRAS, 264, 201

Khochfar S., Silk J., 2006, ApJL, 648, L21

Kormendy J., 1977, ApJ, 218, 333

Mancini C., Daddi E., Renzini A., Salmi F., McCracken H. J., Cimatti A., Onodera M., Salvato M., Koekemoer A. M., Aussel H., Le Floc'h E., Willott C., Capak P., 2010, MNRAS, 401, 933

McIntosh D. H., Bell E. F., Rix H.-W., Wolf C., Heymans C., Peng C. Y., Somerville R. S., Barden M., Beckwith S. V. W., Borch A., Caldwell J. A. R., Häußler B., Jahnke K., Jogee S., Meisenheimer K., Sánchez S. F., Wisotzki L., 2005, ApJ, 632, 191

Mihos J. C., Hernquist L., 1994, ApJL, 437, L47

Naab T., Jesseit R., Burkert A., 2006, MNRAS, 372, 839

Naab T., Johansson P. H., Ostriker J. P., 2009, ArXiv e-prints, astro-ph.CO

Naab T., Khochfar S., Burkert A., 2006, ApJL, 636, L81

Nair P. B., van den Bergh S., Abraham R. G., 2010, ApJ, 715, 606

Nipoti C., Treu T., Bolton A. S., 2008, ArXiv e-prints, 806

Oser L., Ostriker J. P., Naab T., Johansson P. H., Burkert A., 2010, ArXiv e-prints, 1010, 1381

Padmanabhan N., Seljak U., Strauss M. A., Blanton M. R., Kauffmann G., Schlegel D. J., Tremonti C., Bahcall N. A., Bernardi M., Brinkmann J., Fukugita M., Ivezić Ž., 2004, New Astronomy, 9, 329

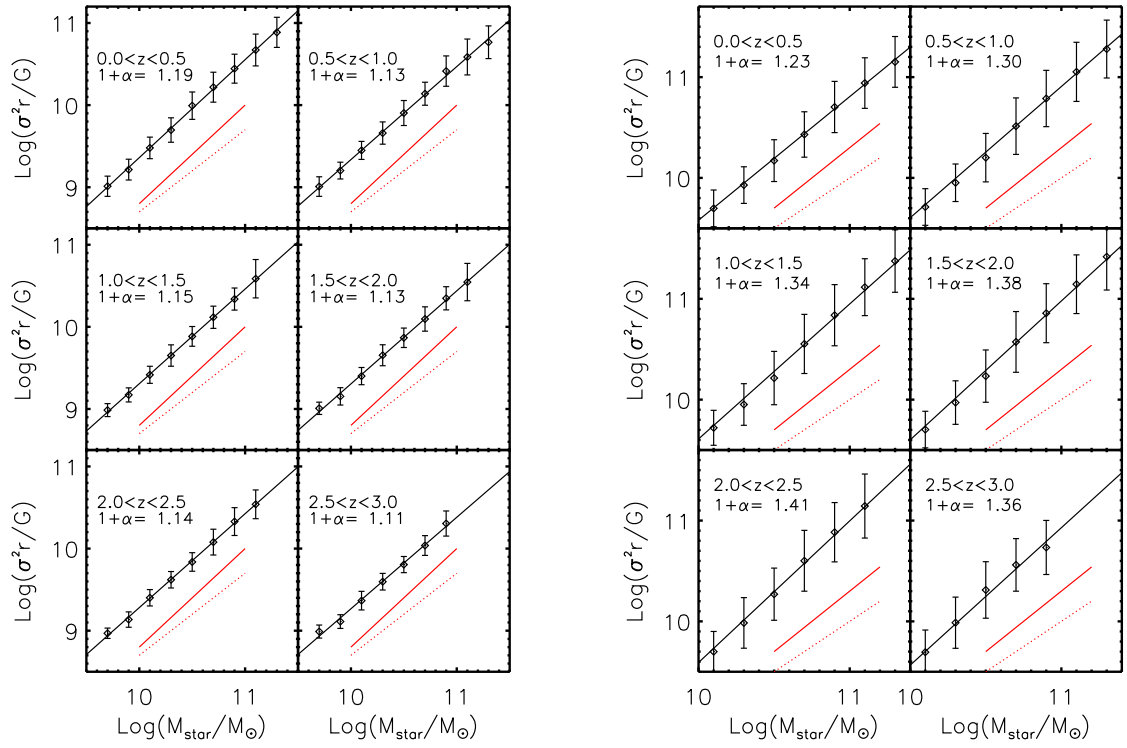

(a) (b)

Figure 14. The fundamental plane produced by the C08 model combined with the new model for central dark matter fractions, applied to S08 (a) and Millennium (b). The tilt in the fundamental plane is larger than created by the new simple model and for both SAMs it is comparable to the observed tilt.

Pahre M. A., Djorgovski S. G., de Carvalho R. R., 1998, AJ, 116, 1591

Robertson B., Bullock J. S., Cox T. J., Matteo T. D., Hernquist L., Springel V., Yoshida N., 2006, ApJ, 645, 986

Robertson B., Cox T. J., Hernquist L., Franx M., Hopkins P. F., Martini P., Springel V., 2006, ApJ, 641, 21

Saglia R. P., Sanchez-Blazquez P., Bender R., Simard L., Desai V., Aragon-Salamanca A., Milvang-Jensen B., Halliday C., Jablonka P., Noll S., Poggianti B., Clowe D. I., Lucia G. D., Pello R., Rudnick G., Valentinuzzi T., White S. D. M., Zaritsky D., 2010, ArXiv e-prints, 1009, 645

Saracco P., Longhetti M., Andreon S., 2009, MNRAS, 392, 718

Shankar F., Marulli F., Bernardi M., Boylan-Kolchin M., Dai X., Khochfar S., 2010, MNRAS, 405, 948

Shankar F., Marulli F., Bernardi M., Dai X., Hyde J. B., Sheth R. K., 2010, MNRAS, 403, 117

Shen S., Mo H. J., White S. D. M., Blanton M. R., Kauffmann G., Voges W., Brinkmann J., Csabai I., 2003, MNRAS, 343, 978

Somerville R. S., Barden M., Rix H.-W., Bell E. F., Beckwith S. V. W., Borch A., Caldwell J. A. R., Häußler B., Heymans C., Jahnke K., Jogee S., McIntosh D. H., Meisenheimer K., Peng C. Y., Sánchez S. F., Wisotzki L., Wolf C., 2008, ApJ, 672, 776

Somerville R. S., Hopkins P. F., Cox T. J., Robertson B. E., Hernquist L., 2008, MNRAS, 391, 481

Somerville R. S., Primack J. R., 1999, MNRAS, 310, 1087

Somerville R. S., Primack J. R., Faber S. M., 2001, MNRAS, 320, 504

Springel V., Hernquist L., 2003, MNRAS, 339, 289

Springel V., Hernquist L., 2005, ApJ, 622, L9

Springel V., White S. D. M., Jenkins A., Frenk C. S., Yoshida N., Gao L., Navarro J., Thacker R., Croton D., Helly J., Peacock J. A., Cole S., Thomas P., Couchman H., Evrard A., Colberg J., Pearce F., 2005, Nature, 435, 629

Springel V., Yoshida N., White S. D. M., 2001, New Astronomy, 6, 79

Tacconi L. J., Genzel R., Neri R., Cox P., Cooper M. C., Shapiro K., Bolatto A., Bouché N., Bournaud F., Burkert A., Combes F., Comerford J., Davis M., Schreiber N. M. F., Garcia-Burillo S., Gracia-Carpio J., Lutz D., Naab T., Omont A., Shapley A., Sternberg A., Weiner B., 2010, Nature, 463, 781

Toomre A., 1977, in Evolution of Galaxies and Stellar Populations Mergers and Some Consequences. p. 401

Toomre A., Toomre J., 1972, ApJ, 178, 623

Trujillo I., Conselice C. J., Bundy K., Cooper M. C., Eisenhardt P., Ellis R. S., 2007, MNRAS, 382, 109

Trujillo et al. 2006, ApJ, 650, 18

van der Wel A., Holden B. P., Zirm A. W., Franx M., Ret-

tura A., Illingworth G. D., Ford H. C., 2008, ApJ, 688, 48
van Dokkum P. G., Whitaker K. E., Brammer G., Franx M., Kriek M., Labbé I., Marchesini D., Quadri R., Bezanson R., Illingworth G. D., Muzzin A., Rudnick G., Tal T., Wake D., 2010, ApJ, 709, 1018
Williams R. J., Quadri R. F., Franx M., van Dokkum P., Toft S., Kriek M., Labbé I., 2010, ApJ, 713, 738
Wuyts S., Cox T. J., Hayward C. C., Franx M., Hernquist L., Hopkins P. F., Jonsson P., van Dokkum P. G., 2010, ApJ, 722, 1666
York D. G., Adelman J., Anderson Jr. J. E., Anderson S. F., Annis J., Bahcall N. A., Bakken J. A., Barkhouser R., Bastian S., Berman E., Boroski W. N., Yanny B., Yasuda N., 2000, AJ, 120, 1579
Zaritsky D., Zabludoff A. I., Gonzalez A. H., 2007, ArXiv e-prints, 711

7 APPENDIX A: NEW MODEL FOR CENTRAL DARK MATTER FRACTION

In C08 we presented a formula for calculating the dark matter fraction in the central part of the merger remnants. We define the dark matter fraction with a given radius as

$$f_{\rm dm} = \frac{M_{\rm dm}}{(M_{\rm dm} + M_{\rm stars})}, \quad (15)$$

where $M_{\rm dm}$ and $M_{\rm stars}$ are the dark matter and stellar masses inside that radius, respectively. For the merger simulations we found that the dark matter fraction inside half of the stellar half mass radius could be well-approximated by the following formula:

$$f_{\rm dm,f} = \frac{M_{\rm dm,1} + M_{\rm dm,2}}{M_{\rm dm,1} + M_{\rm dm,2} + C_{\rm stars}(M_1 + M_2 + M_{\rm new})}. \quad (16)$$

$M_{\rm dm,1}$ and $M_{\rm dm,2}$ are the dark matter masses inside half of the three-dimensional stellar half-mass radii of the progenitors, M_1 and M_2 are the total stellar masses of the progenitors, and $M_{\rm new}$ is the total mass of stars formed during the merger. This expression simply assumes that the inner region of the remnant contains the same amount of dark matter as the sum of the inner regions of the progenitors, and that a fixed fraction, $C_{\rm stars}$, of the final stellar mass is inside one-half of the three-dimensional stellar half-mass radius.

While this formula works well for the simulated remnants, it fails outside the regime where $R_{progenitor} \sim R_{remnant}$. One of the benefits of the formula is that since it puts all of the central dark matter from the progenitors into the central portion of the remnant it allows contraction of the halo as a result of the baryonic dissipation. However, this contraction is precisely what causes the problem when the initial and final radii differ greatly. Specifically, for high gas fraction progenitors with large radii, the remnants can have much smaller radii and the previous formula predicts extreme contraction of the dark matter.

In order to increase the range of applicability of the merger model, we introduce a simpler, more physically intuitive model for predicting the central dark matter fraction that does not suffer from the deficiencies mentioned above. We begin with the dark matter halo masses and half-mass radii, and assume that the two halos merge dissipationlessly so that

$$\frac{(M_{1,\rm dm} + M_{2,\rm dm})^2}{R_{\rm dm,f}} = \frac{M_{1,\rm dm}^2}{R_{1,\rm dm}} + \frac{M_{2,\rm dm}^2}{R_{2,\rm dm}}. \quad (17)$$

This equation can be solved for the final halo half-mass radius ($R_{\rm dm,f}$). We use the final radius and mass to fit an isothermal profile to the final halo. Then we calculate the mass expected inside the stellar half-mass radius and this value is used to calculate the final central dark matter fraction. For this paper we calculate the dark matter fraction inside the stellar half-mass radius and use this to compute the velocity dispersion of the merger remnant. In addition to extending the range of validity, this new method removes one of the least certain parameters from the merger model. A check against the merger simulations demonstrates that the new method produces a larger scatter between predicted and measured velocity dispersion, with the fractional rms scatter increasing from 0.24 to 0.35. However, most of the additional scatter results from variations in orbit, and in this work we find that the distribution of orbits found in N-body simulations is such that orbital variation plays a minor role.